# Old open clusters and the Galactic metallicity gradient: Berkeley 20, Berkeley 66, and Tombaugh 2\*

Gloria Andreuzzi<sup>1,2</sup>†, Angela Bragaglia<sup>3</sup>, Monica Tosi<sup>3</sup> and Gianni Marconi<sup>4</sup>

- <sup>1</sup> Fundación Galileo Galilei INAF, Rambla José Ana Fernández Pérez, 7, 38712 Breña Baja, TF (Spain)
- <sup>2</sup> INAF-Osservatorio Astronomico di Roma, Via dell'Osservatorio 5, I-00040 Monte Porzio (Italy)
- <sup>3</sup> INAF-Osservatorio Astronomico di Bologna, Via Ranzani 1, I-40127 Bologna (Italy)
- <sup>4</sup> ESO, Alonso de Cordova 3107, Vitacura, Santiago, Chile

#### ABSTRACT

To study the crucial range of Galactocentric distances between 12 and 16 kpc, where little information is available, we have obtained VI CCD imaging of Berkeley 20 and BVI CCD imaging of Berkeley 66 and Tombaugh 2, three distant, old open clusters. Using the synthetic colour magnitude diagram (CMD) technique with three types of evolutionary tracks of different metallicities, we have determined age, distance, reddening and indicative metallicity of these systems. The CMD of Be 20 is best reproduced by stellar models with a metallicity about half of solar (Z=0.008 or 0.01), in perfect agreement with high resolution spectroscopic estimates. Its age  $\tau$  is between 5 and 6 Gyr from stellar models with overshooting and between 4.3 and 4.5 Gyr from models without it. The distance modulus from the best fitting models is always (m-M)<sub>0</sub>=14.7 (corresponding to a Galactocentric radius of about 16 kpc), and the reddening E(B-V) ranges between 0.13 and 0.16. A slightly lower metallicity  $(Z \simeq 0.006)$  appears to be more appropriate for Be 66. This cluster is younger,  $\tau=3$  Gyr, and closer, (m-M)<sub>0</sub>=13.3 (i.e., at 12 kpc from the Galactic centre), than Be 20, and suffers from high extinction,  $1.2 \le E(B-V) \le 1.3$ , variable at the 2-3 per cent level. Finally, the results for To 2 indicate that it is an intermediate age cluster, with  $\tau$  about 1.4 Gyr or 1.6-1.8 Gyr for models without and with overshooting, respectively. The metallicity is about half of solar (Z=0.006 to 0.01), in agreement with spectroscopic determinations. The distance modulus is (m-M)<sub>0</sub>=14.5, implying a distance of about 14 kpc from the Galactic centre; the reddening E(B-V) is 0.31-0.4, depending on the model and metallicity, with a preferred value around

**Key words:** Galaxy: disc – Hertzsprung-Russell (HR) diagram – open clusters and associations: general – open clusters and associations: individual: Berkeley 20, Berkeley 66, Tomabugh 2

# 1 INTRODUCTION

Open clusters (OCs) are very good tracers of the Galactic disc properties, of its formation and evolution (e.g. Panagia & Tosi 1981; Friel 1995; Twarog, Ashman, & Anthony-Twarog 1997; Freeman & Bland-Hawthorn 2002). In particular, OCs can be used to study the metallicity distribution in the disc and its possible evo-

† E-mail: andreuzzi@tng.iac.es (GA), angela.bragaglia@oabo.inaf.it (AB), monica.tosi@oabo.inaf.it (MT) gmarconi@eso.org (GM)

lution with time. With the BOCCE (Bologna Open Cluster Chemical Evolution) project, described in detail by Bragaglia & Tosi (2006), we are deriving precise and homogeneous ages, distances, reddenings and chemical abundances for a large sample of OCs. The final goal is to study the present status of the Galactic disc, its formation and evolution. Since the least known epochs of the disc evolution are the earliest ones, we put particular attention to the study of old clusters. Adding the present three old systems to those already described in Bragaglia & Tosi (2006), to Be 17 (Bragaglia et al. 2006a), Be 32 and King 11 (Tosi, Bragaglia & Cignoni 2007), we have already examined 17 clusters older than 1 Gyr, out of the about 190 listed in the Dias et al. (2002) catalogue.

As part of this project, we present here a photometric study of three clusters: (a) Berkeley 20 ( $l=203.^{\circ}48, b=-17.^{\circ}37,$ 

<sup>\*</sup> Based on observations made with the Italian Telescopio Nazionale Galileo (TNG) operated on the island of La Palma by the Fundación Galileo Galilei of the INAF (Istituto Nazionale di Astrofisica) at the Spanish Observatorio del Roque de los Muchachos of the Instituto de Astrofisica de Canarias, and on observations obtained at the ESO telescopes in La Silla (Chile) under programmes 67.D-0014, 68.D-0222

in the third Galactic quadrant); (b) Berkeley 66 ( $l=139.^\circ43$ ,  $b=0.^\circ22$ , in the second Galactic quadrant); and (c) Tombaugh 2 ( $l=232.^\circ83$ ,  $b=-6.^\circ88$ , in the third Galactic quadrant). They are old, distant clusters, and their properties are important to understand the nature of the outer Galactic disc. In fact, they all lie in the region between about 12 and 16 kpc from the Galactic centre, where the radial metallicity distribution seems to change its slope (see Sect. 6). Furthermore, To 2 has been connected with the Monoceros ring and the Canis Major overdensity (e.g., Frinchaboy et al. 2004; Bellazzini et al. 2004, see also Sect. 2.3).

Our paper is organized as follows: in Sect. 2 we give a short description of what is already available on these clusters in literature, while in Sect. 3 we describe our data and the reduction procedure. In Sect. 4 we present the CMDs and in Sect. 5 we detail the cluster parameter derivation. Finally, Sect. 6 is dedicated to a summary and discussion, in particular of the radial Galactocentric metallicity gradient and the importance of the three clusters in this context.

#### 2 THE THREE CLUSTERS IN THE LITERATURE

The three clusters have already been partly studied in the past and we briefly summarise here the available information. We have retrieved (from the WEBDA<sup>1</sup> or the original papers) the values of radial velocity (RV) for stars in our catalogues. They are presented in Tables 1, 2, and 3, together with photometric data, coordinates, and identifications. The information on membership and metallicity (see next) for the clusters will be used in the present paper to help in the selection of the best-fitting synthetic CMDs.

#### 2.1 Be 20

The first calibrated photometry for Be 20 was presented by MacMinn et al. (1994), who obtained V,I data on a  $5.1\times5.1$  arcmin² field using the KPNO 2.1m telescope. Their CMD is well defined, but shows an apparent lack of red clump (RC) stars. MacMinn et al. (1994) derived, using isochrones, an age of 6 Gyr, [Fe/H] $\simeq -0.23$ ,  $(m-M)_V \simeq 15.0$  and  $E(V-I) \simeq 0.16$ . They deduced a radius of 1.5 arcmin and a mass of about  $1000~{\rm M}_\odot$ . They considered Be 20 worth of further interest also because of its large Galactocentric distance (R $_{GC} \simeq 15.8~{\rm kpc}$ ) and unusual position below the Galactic plane (about 2.5 kpc).

Durgapal, Pandey, & Mohan (2001) presented B,V,R,I data obtained at the 104-cm Naini Tal State Observatory over a  $6\times 6$  arcmin² field. At variance with the other photometric works, they do think they see a horizontal branch in the innermost region of Be 20. Using two different sets of isochrones they concluded for an age of about 5 Gyr, E(B-V)=0.10, Z=0.008 (i.e. [Fe/H] $\simeq -0.3$ ),  $(m-M)_V\simeq 15.1$ , a cluster radius of about 2.5 arcmin and a  $R_{GC}\simeq 17.1$  kpc.

Momany et al. (2001) showed results on B,V photometry obtained with the Wide Field Imager (WFI@2.2m ESO-Max Planck telescope) on a much larger field of view (about  $30\times30~{\rm arcmin^2}$ ). These observations were intended to produce catalogues over fields of view appropriate to the FLAMES fiber spectrograph and the authors did not really discuss the cluster properties.

Radial velocities (see Table 1) and abundances based on

low resolution spectroscopy were presented by Friel et al. (2002) for nine stars; six of them appear to be cluster members and have  $\langle RV \rangle = +70 \pm 13 \text{ km s}^{-1}$ , [Fe/H]= $-0.61 \pm 0.14 \text{ dex}$ . Frinchaboy et al. (2006) observed 20 objects in Be 20 at intermediate resolution and derived precise RVs; only five stars resulted members and their average RV is  $+75.7 \pm 2.4 \text{ km s}^{-1}$ .

Abundances based on high resolution spectroscopy were first measured by Yong, Carney, & Teixera de Almeida (2005). They observed four stars, two in common with Friel et al. (2002), one with Frinchaboy et al. (2006); their average RV is  $+78.9\pm0.7$  km s<sup>-1</sup>. Abundance analysis was possible only for two stars, located near the RGB tip, giving [Fe/H] $\simeq -0.49\pm0.06$  dex. Yong et al. (2005) derived detailed abundances and discussed this cluster in the framework of Galactic abundance trends and different origin/population. Finally, Sestito et al. (2008) obtained FLAMES/UVES spectra of six stars in the field of Be 20 over the large WFI area; two of them are confirmed cluster members, and their analysis gives a metallicity [Fe/H]=-0.3 (rms=0.02) dex.

#### 2.2 Be 66

For Be 66, the only available photometry reaching the main sequence Turn-Off (MSTO) is by Phelps & Janes (1996). They observed a  $5.1\times5.1$  arcmin² field using the KPNO 2.1m telescope with the V,I filters, obtaining a well defined CMD. They derived the following parameters: age =  $3.5\pm1.0$  Gyr,  $-0.23\leqslant [{\rm Fe/H}]\leqslant 0, E(V-I)=1.60\pm0.05, (m-M)_V=17.40\pm0.20$  (implying a Galactocentric distance  $R_{GC}\simeq12.9$  kpc), radius of 1.2-3.5 arcmin and minumum mass of  $\sim750~{\rm M}_{\odot}$ ; they also suggested the possibility of differential reddening.

Villanova et al. (2005) obtained high resolution spectra of two red clump stars with the HIRES spectrograph on the Keck I telescope. They have RVs -50.6 and -50.7 km s<sup>-1</sup> (see Table 2), and seem to be cluster members. Abundance analysis was possible only for one star; Villanova et al. estimated [Fe/H]=  $-0.48 \pm 0.24$  and claimed that other elements have solar scaled ratios.

#### 2.3 To 2

Although with significant discrepancies, all authors concur that To 2 is a distant, old, rather metal-poor open cluster. To 2 was discovered by Tombaugh (1938) and its first CMD, barely reaching the main sequence turn-off, was published by Adler & Janes (1982). B, V, I images were collected with a variety of cameras at the 1m and 2.5-m telescopes in Las Campanas by Kubiak et al. (1992), who intended to find variable stars. Their CMDs are of very good quality (see also Sect. 3.2) and they derive a distance of  $6.3 \pm 0.9$ kpc and an age of 4 Gyr, assuming E(V-I) = 0.4 and a metallicity one tenth of solar. Phelps et al. (1994) included To 2 in their list of old OCs, assigning it a value of  $\delta V = 1.5$ , i.e., an age of about 2.5 Gyr (following the formula in Janes & Phelps 1994). No further photometric catalogues are freely available, but Villanova et al. (2010) re-determined the parameters of To 2 on the basis of spectroscopy (see below) and photometry, deriving an age of 2 Gyr,  $(m-M)_V = 15.1$ , E(B-V) = 0.25, with [Fe/H]=-0.32 dex (see next).

The metallicity of this cluster has been determined using low-resolution spectroscopy by Friel et al. (2002), who find [Fe/H]=  $-0.4\pm0.09$  using 12 stars; the corresponding RVs are given in Table 3, together with the ones by others, for all stars in common with our photometric catalogue. Brown et al. (1996) analysed

<sup>&</sup>lt;sup>1</sup> http://www.univie.ac.at/webda/webda.html, see Mermilliod & Paunzen (2003)

**Table 1.** Stars in our Be 20 photometric catalogue for which RVs have been published. FLAMES stands for the RVs from Sestito et al. (2007). ID in first column is our identificator;  $ID_1$ ,  $ID_2$  are in the WEBDA system;  $ID_3$  is taken directly from the Frinchaboy et al. (2006) paper. The precision of the velocities is 0.5, 10, 1, 2 km s<sup>-1</sup> for RV<sub>0</sub>, RV<sub>1</sub>, RV<sub>2</sub> and RV<sub>3</sub>, respectively.

ID	V	I	RA(2000) hh:mm:ss	DEC(2000) dd:pp:ss	FLAMES RV <sub>0</sub>	Friel e ID <sub>1</sub>	t al. 2002 RV <sub>1</sub>	Yong e	et al. 2005 RV <sub>2</sub>	Frinchabo	y et al. 2006 RV <sub>3</sub>	member
822	14.792	13.325	05:32:37.957	+00:11:09.61				5	77.3	10770	75.5	Y
843	15.145	13.749	05:32:38.960	+00:11:20.33	78.6	_	_	8	78.9	_	-	Y
28	15.750	14.565	05:32:39.228	+00:10:31.04		10	82	_	_	10810	63.7	Y
354	16.922	15.752	05:32:36.886	+00:11:49.49		22	84	22	78.9	_	73.7	Y
185	17.080	15.928	05:32:33.213	+00:09:34.79		27	15	_	_	10617	0.1	N
395	16.841	16.023	05:32:42.328	+00:12:29.39		29	61	_	_	_	_	Y
368	17.446	16.312	05:32:37.014	+00:12:00.54		33	54	_	_	10741	74.5	Y
281	17.543	16.442	05:32:33.276	+00:10:53.32		37	69	_	_	_	_	Y
780	17.496	16.492	05:32:33.509	+00:11:37.62		39	69	_	_	_	_	Y
137	17.613	16.534	05:32:46.573	+00:08:41.92		_	_	_	_	10940	40.2	N
396	19.291	17.687	05:32:41.827	+00:12:29.98		_	_	_	_	10864	30.8	N
72	17.040	15.960	05:32:34.739	+00:15:38.72		_	_	_	_	10645	24.4	N
179	16.939	16.205	05:32:39.000	+00:09:27.31		_	_	_	_	10806	35.3	N
48	16.584	15.697	05:32:50.012	+00:11:54.12		_	_	_	_	10979	32.5	N
991	19.064	17.739	05:32:50.735	+00:16:12.99		_	_	_	_	10980	53.8	N
74	15.919	14.673	05:32:46.420	+00:15:52.23	85.4	_	_	_	_	_	_	N?
702	16.187	14.943	05:32:36.774	+00:11:04.84	78.5	11	_	_	_	_	_	Y
977	15.447	13.992	05:32:50.067	+00:16:16.59	37.7	-	-	-	-	_	_	N

Table 2. RVs for the two stars (both members) in Be 66 analysed by Villanova et al. (2005). ID, magnitudes, and coordinates are from our work.

ID	$ID_{\mathrm{WEBDA}}$	В	V	Ι	RA(2000) hh:mm:ss	DEC(2000) dd:pp:ss	RV km s <sup>-1</sup>
6521	785	20.375	18.232	15.596	03:04:02.90	+58:43:57.0	$-50.7 \pm 0.1$
5793	934	20.357	18.217	15.595	03:04:06.41	+58:43:31.0	$-50.6 \pm 0.3$

high-resolution spectra of three stars, finding an average [Fe/H]=  $-0.4\pm0.25$  (with E(B-V)=0.4), and rather normal elemental ratios (e.g., slightly enhanced  $\alpha\text{-elements}$ , slightly deficient oxygen) although with a caveat on the uncertainties.

This cluster could even be of extragalactic origin, and only recently accreted by the Milky Way: on the basis of positional and kinematical arguments, Frinchaboy et al. (2004) proposed that To 2 is part, together with other OCs, of the Monoceros stream, also called GASS, Great Anticenter Stellar Stream (Newberg et al. 2002; Ibata et al. 2003), possibly due to a dissolving, merging galaxy. Bellazzini et al. (2004) associated To 2 directly to the dissolving dwarf galaxy proposed as origin of the Monoceros stream (Martin et al. 2004), i.e., to Canis Major (CMa), whose reality has however been questioned by others (e.g., Momany et al. 2004). To 2 has then attracted the attention of several groups and two papers on its metallicity have recently appeared.

Frinchaboy et al. (2008) analysed high-resolution UVES and GIRAFFE VLT spectra of 40 stars, of which only about one half turned out to be members on the basis of the RVs. Their surprising results is the presence of two sub-populations, both apparently member of the cluster, one more metal-poor,  $\alpha$ -rich ([Fe/H=-0.28, [Ti/Fe]=+0.36, seven stars) and more centrally concentrated, the other more metal-rich, with solar-scaled  $\alpha$  elements ([Fe/H=-0.06, [Ti/Fe]=+0.02, 11 stars) and more external. If confirmed, it would be the first case of chemical inhomogeneity in OCs and maybe of multiple stellar generations. To 2 would in any case represent a very different case from globular clusters

(GCs). There, inhomogeneities, initially regarded as "anomalies", have been found since a long time, but only in light elements, like C, N, O, Na, etc, whose abundance variations are (anti-)correlated (Gratton, Sneden, & Carretta 2004). In contrast, the metallicity of GCs, described by [Fe/H], is homogeneous to better than 10 per cent (Carretta et al. 2009), with very few exceptions, like  $\omega$  Centauri, or M22. While the presence of multiple stellar generations in (probably all) GCs is presently widely accepted and is based on both photometric and spectroscopic evidence (see, e.g., Bragaglia 2010), the mass of GCs is much higher than that of OCs, and mass is certainly of paramount importance in shaping the destiny of a cluster. To explain the peculiar case of To 2, Frinchaboy et al. (2008) proposed several alternative solutions: two overlapping, or merged, clusters, multiple star formation periods, or the presence of both an open cluster and a stream, remnant of the same dwarf galaxy where also To 2 was born.

This result has however been questioned by part of the same team; Villanova et al. (2010) presented results on GIRAFFE VLT spectra for 37 RGB and red clump stars (only 15 actually members, and only 13 with data good enough for the analysis). They found [Fe/H]=  $-0.31\pm0.02$  dex (rms=0.07 dex) and *no* sign of a bimodal distribution. All the other measured elements are also uniform. They discuss the cause of this very discrepant result and the only reasonable explanation appears to be the better quality of the new data and the fact that their spectra are in a redder region than the Frinchaboy et al. (2008) ones, hence more easily analysed for

# 4 Andreuzzi et al.

Table 3. RVs for stars in To 2. ID, magnitudes, and coordinates are from our work. RV $_1$ : Brown et al 1996; RV $_2$ : Friel et al. 2002; RV $_3$ : Frinchaboy et al. 2008; ID $_4$  and RV $_4$ : Villanova et al. (2010) (their Tables 1 and 5).

1476	ID	$ID_{WEBDA}$	В	V	I	RA (2000) hh:mm:ss	Dec (2000) dd:pp:ss	$\begin{array}{c} \text{RV}_1 \\ \text{km s}^{-1} \end{array}$	$\begin{array}{c} \rm RV_2 \\ \rm km~s^{-1} \end{array}$	$ m RV_3$ $ m km~s^{-1}$	$ID_4$	$RV_4$ km s <sup>-1</sup>	Member?
1224   1236   1236   1238   13628   12344   0793/210398   20-047-1144   123.0	4736	0007	13.974	12.893	11.654	07:02:58.281	-20:43:54.15	117.2					Y
17.2   17.2	2272		15.293	13.401		07:03:06.329	-20:50:07.95	113.9					
1888   1889													
1.450								117.2					
2278   0028													
2348   0047													
2358   0056   16,044   48,65   13,91   07,025,025   20,045,219   131,0													
2358   0056   16.044   14.865   15.91   07.03.009.35   20.452.194   131.0   Y   Y   2355   20.55.294.0   14.20   Y   Y   2356   0057   15.378   14.845   14.20   07.024.7275   20.55.294.0   14.20   Y   Y   2294   0062   15.379   15.058   14.273   07.025.393   20.505.54.2   139.0   Y   Y   Y   Y   Y   Y   Y   Y   Y													
1.55													
2360   0058   15.990   14.897   15.693   107.03.00.169   20.45.18.48   117.0   Y   Y   Y   2294   0062   15.537   15.073   14.530   07.03.10.1692   20.48.29.87   129.0   Y   Y   2385   0076   16.622   15.161   13.898   07.03.23.050   20.53.28.889   84.9   Y   Y   Y   2385   0076   16.622   15.161   13.898   07.03.23.050   20.53.28.889   84.9   X   Y   Y   Y   Y   Y   Y   Y   Y   Y													
2299													
2294   0062   15.537   15.073   14.530   07/03-10.992   20-48/29.87   129.0   Y   Y   2-224   20.063   16.482   15.562   13.896   07/03-23.050   20-53.38.89   84.9   N   N   2288   0080   16.282   15.355   13.816   07/03-24.744   20-522.882   90.6   16.99   90.0   N   2299   0089   16.680   15.468   14.036   07/03-15.411   20-522.882   90.6   16.99   90.0   N   2402   0096   16.840   15.565   14.113   07/03-20.364   20-455.55.77   127.7   N   N   2180   0097   16.982   15.552   13.935   07/03-19.799   20-51.5241   10.58   N   N   2188   0098   16.919   15.557   14.014   07/03-09.236   20-455.55.77   127.7   Y   Y   2165   0102   16.646   15.689   14.366   07/03-05.666   20-49/3-0.670   122.0   Y   Y   2412   0106   16.744   15.675   14.494   07/03-21.766   20-54-08.13   43.4   N   2413   0107   16.890   15.751   14.242   07/03-01.871   07/03-13.89   20-54-08.13   43.4   N   2413   0107   16.890   15.731   14.22   07/03-13.710   20-52-58.44   74.4   16.0   74.5   N   2413   0101   17.049   15.731   14.22   07/03-13.710   20-52-58.44   74.4   16.0   74.5   N   2434   0115   16.856   15.699   14.550   07/03-12.533   20-49-26.82   39.0   21.8   Y   2434   0126   17.065   15.911   14.579   07/02-55.195   20-49-20.80   12.18   Y   2436   0127   17.188   15.947   14.526   07/02-55.195   20-49-20.80   12.18   Y   2444   0141   17.119   15.999   147.49   07/03-27.196   20-49-20.80   12.12   28   20-49-20.80   12.12   28   20-49-20.80   12.12   28   20-49-20.80   12.12   28   20-49-20.80   12.12   28   20-49-20.80   12.12   28   20-49-20.80   12.12   28   20-49-20.80   12.12   28   20-49-20.80   12.12   28   20-49-20.80   12.12   28   20-49-20.80   12.12   28   20-49-20.80   12.12   28   20-49-20.80   12.12   20-49-20.80   12.12   20-49-20.80   12.12   20-49-20.80   12.12   20-49-20.80   12.12   20-49-20.80   12.12   20-49-20.80   12.12   20-49-20.80   12.12   1													
2388   0076   16.622   15.316   13.898   07/03/23/050   20.553/88.89   84.9	2294			15.073	14.530		-20:48:29.87		129.0				
2388   0080	2174	0063	16.413	15.062	13.590	07:03:06.851	-20:48:28.12			121.0			Y
2299   0089   16.680   15.468   14.036   07:03:15.411   -20:52:25.82   90.6   16.99   90.0   N	2385		16.622	15.316	13.898	07:03:23.050	-20:53:38.89			84.9			N
2402   0096   16.840   15.555   14.113   0703.20.364   -20.45.55.57   127.7   N   N   12180   0097   16.982   15.552   13.935   0703.197.59   20.51.52.41   105.8   N   N   12180   0098   16.919   15.557   14.014   07.03.09.236   -20.51.28.99   121.7   Y   Y   Y   12165   0102   16.646   15.689   14.366   07.03.06.566   -20.49.36.70   122.0   Y   Y   Y   12181   0106   16.744   15.675   14.949   07.03.21.766   -20.54.08.13   43.4   N   N   14.34   16.07   14.949   07.03.21.766   -20.54.08.13   43.4   N   N   Y   Y   Y   Y   Y   Y   Y   Y													
2180											169	90.0	
2158   0098   16.919   15.557   14.014   07.03.09.236   -20.51.28.99   121.7   Y   2412   0106   16.744   15.675   14.494   07.03.05.266   -20.49.36.70   122.0   Y   2413   0107   16.800   15.677   14.394   07.02.21.766   -20.540.81.3   43.4   N   N   2413   0107   16.800   15.752   14.394   07.02.25.38.80   -20.46.39.11   93.2   N   2417   0109   16.992   15.732   14.372   07.03.06.117   -20.550.30.77   122.1   299   121.8   Y   41.633   0110   17.049   15.731   14.242   07.03.06.117   -20.503.077   122.1   299   121.8   Y   41.633   0115   16.856   15.769   14.555   07.03.06.117   -20.503.077   122.1   299   121.8   Y   41.633   0115   16.856   15.769   14.555   07.03.02.12.533   -20.49.26.82   39.0   20.6   1886   120.0   Y   2434   0126   17.065   15.911   14.579   07.02.55.195   -20.49.20.80   120.6   1886   120.0   Y   2434   0126   17.105   15.911   14.579   07.02.55.195   -20.49.20.80   120.6   1886   120.0   Y   2436   0127   17.188   15.947   14.572   07.02.53.932   -20.50.09.69   119.2   1672   119.1   Y   4.693   0140   17.121   15.979   14.572   07.02.53.932   -20.50.09.69   119.2   1672   119.1   Y   2444   0141   17.119   15.969   14.719   07.02.51.15   -20.471.5.09   10.40   2343   104.0   N   2446   0142   17.132   15.990   14.734   07.03.07.69   -20.521.978   10.11   18.8   Y   2463   0158   17.273   16.124   14.739   07.03.07.69   -20.46.17.21   118.8   Y   2463   0158   17.273   16.124   14.739   07.03.07.69   -20.46.17.21   118.8   Y   2463   0158   17.273   16.124   14.799   07.03.07.60   -20.46.17.57   118.0   118.7   Y   2444   0179   17.411   16.243   14.836   07.03.07.68   -20.46.17.57   122.6   591   125.1   Y   2444   0179   17.411   16.243   14.897   07.03.07.60   -20.44.51.57   122.6   591   125.1   Y   2444   0179   17.411   16.243   14.897   07.03.07.60   -20.44.51.57   122.6   59.1   125.1   Y   2449   07.03.07.60   -20.44.51.57   22.6   591   125.1   Y   2449   07.03.07.60   -20.44.51.57   22.6   591   125.1   Y   2449   07.03.07.60   -20.44.51.57   22.6   591   125.1   Y   2													
2412   0106													
2412   0106													
2413         0107         16,800         15,677         14,344         0702,53,880         -20-46,39,11         93.2         N           2417         0109         16,992         15,732         14,372         0703,513,710         -20-50,30,77         122,1         299         121.8         Y           2183         0110         17,049         15,731         14,242         0703,06,117         -20-50,30,77         122,1         299         121.8         Y           270         0124         17,184         15,964         14,460         0703,02,89         20-50,00,82         121.8         Y           2436         0126         17,065         15,911         14,579         0702,55,195         -20-50,00,82         121.8         8         120.0         Y           2436         0127         17,188         15,947         14,526         070,255,978         -20-500,969         119.2         1672         119.1         Y           42439         0135         17,169         15,951         14,526         070,259,793         -20-50,00,69         119.2         1672         119.1         Y           24439         0140         17,132         15,994         14,734         070,259,733         -20-49,3													
2417   0109   16,992   15,732   14,372   07,0316,710   20,52,5844   74,4   160   74,5   N     2183   0110   17,049   15,731   14,242   07,0306,117   20,5030,777   12,1   299   121,8   Y     1463   0115   16,856   15,769   14,565   07,031,2533   20,49,26,82   39,0   N     270   0124   17,184   15,904   14,460   07,032,07,289   20,50,00,82   121,8   Y     2434   0126   17,655   15,911   14,579   07,02,55,197   20,49,20,80   120,6   18,86   120,0   Y     2436   0127   17,188   15,947   14,526   07,02,55,478   20,511,543   121,1   238   120,5   Y     2439   0135   17,169   15,961   14,551   07,02,55,1928   20,500,969   119,2   1672   119,1   Y     2441   0141   17,119   15,969   14,734   07,02,51,115   20,47,15,09   104,0   2343   104,0   N     2446   0142   17,132   15,990   14,734   07,03,27,926   20,52,19,78   101,1   N     2446   0146   17,207   16,051   14,684   07,03,09,695   20,45,48,97   119,5   Y     2450   0146   17,207   16,051   14,684   07,03,09,695   20,46,47,57   118,8   Y     755   0162   17,273   16,123   14,386   07,03,01,582   20,46,47,57   122,6   591   125,1   Y     2424   0165   17,364   16,169   14,776   07,03,01,582   20,46,47,57   122,6   591   125,1   Y     2424   0179   17,411   16,243   14,876   07,03,01,582   20,46,47,57   122,6   591   125,1   Y     2424   0179   17,411   16,243   14,876   07,03,01,582   20,46,47,57   122,6   591   125,1   Y     2424   0190   17,311   16,285   15,099   07,02,52,139   20,48,318   117,2   Y     2424   0190   17,410   16,256   14,928   07,03,01,582   20,48,57,53   118,0   Y     2424   0190   17,516   16,256   14,928   07,03,00,647   20,49,42,05   123,7   Y     2424   0190   17,516   16,360   14,910   07,02,53,102   20,48,31,7   80,6   N     2424   0196   17,557   16,381   14,915   07,02,53,139   20,48,39,33   32,0   N     2439   0201   17,463   16,380   14,915   07,02,53,859   20,48,39,33   32,0   N     2449   0219   17,516   16,497   15,595   15,299   07,03,50,617   20,49,07,82   121,5   35,74   121,7   Y     2489   0217   17,411   16,589   15,099   07													
2183   0110											160	74.5	
1463   0115													
270         0124         17.184         15.904         14.460         07.03.07.289         -20.05.00.82         121.8         Y           2434         0126         17.065         15.911         14.579         07.02.55.195         -20.49.20.80         120.6         1886         120.0         Y           2439         0135         17.169         15.961         14.551         07.02.53.928         -20.50.09.69         119.2         1672         119.1         Y           2431         0140         17.215         15.974         14.572         07.02.59.78         -20.49.33.36         121.2         Y           2441         0141         17.119         15.969         14.719         07.02.59.715.15         -20.4715.09         104.0         2343         104.0         N           2441         0141         17.132         15.990         14.734         07.03.27.768         -20.451.78         101.1         N         N         2450         0146         17.273         16.121         14.836         07.03.30.758         -20.461.721         118.8         Y         Y         755         0162         17.273         16.147         14.799         07.03.30.1582         -20.477.59.53         118.0         Y         24.51													
2436         0127         17.188         15.947         14.526         07:02:55.478         -20:51:15.43         121.1         238         120.5         Y           2439         0135         17.169         15.961         14.551         07:02:55.788         -20:50:00-69         119.2         1672         119.1         Y           693         0140         17.215         15.974         14.572         07:02:59.788         -20:49:33.36         121.2         Y           2441         0141         17.119         15.969         14.719         07:02:51.115         -20:47:15.09         104.0         2343         104.0         N           2446         0142         17.132         15.990         14.734         07:03:27.926         -20:45:19.78         101.1         N         N           2450         0146         17.207         16.051         14.684         07:03:09.69         -20:45:48.89         119.5         Y         Y           2463         0158         17.273         16.123         14.836         07:03:01.182         -20:45:17.21         118.8         Y         Y           2556         0162         17.341         16.104         14.779         07:03:03:13         20:47:59:53         1	270	0124	17.184	15.904	14.460	07:03:07.289	-20:50:00.82						
2439         0135         17,169         15,961         14,551         07:02:53,928         -20:50:09:69         119.2         1672         119.1         Y           693         0140         17,215         15,974         14,572         07:02:59:738         -20:49:33.36         121.2         Y           2441         0141         17,119         15,969         14,719         07:02:51.115         -20:47:15:09         104.0         2343         104.0         N           2446         0142         17.132         15.990         14.734         07:03:27.926         -20:52:19.78         101.1         N         N           2450         0146         17.207         16.051         14.684         07:03:07.768         -20:46:17.21         118.8         Y           755         0162         17.273         16.123         14.836         07:03:01.582         -20:47:59.53         118.0         Y           556         0164         17.347         16.170         14.759         07:03:20.483         -20:46:47.57         122.6         591         125.1         Y           268         0177         17.379         16.243         14.876         07:03:07.204         -20:50:20.41         118.7         Y	2434	0126	17.065	15.911	14.579	07:02:55.195	-20:49:20.80			120.6	1886	120.0	Y
693         0140         17.215         15.974         14.572         07:02:59.738         -20:49:33.36         121.2         Y           2441         0141         17.119         15:969         14.719         07:02:51.115         -20:47:15:09         104.0         2343         104.0         N           2446         0142         17.132         15:990         14.734         07:03:27.926         -20:52:19.78         101.1         N         N           2450         0146         17.207         16:051         14.684         07:03:09.695         -20:45:48.97         119.5         Y           2463         0158         17.273         16:147         14.799         07:03:07.768         -20:46:17.21         118.8         Y           755         0162         17.273         16:142         14.876         07:03:01.582         -20:46:17.55         118.0         Y           556         0164         17.347         16:170         14.759         07:03:03.513         -20:46:47.57         122.6         591         125.1         Y           268         0177         17.379         16:243         14.876         07:03:03.513         -20:46:47.57         122.6         591         125.1         Y													
2441         0141         17.119         15.969         14.719         07:02:51.115         -20:47:15.09         104.0         2343         104.0         N           2446         0142         17.132         15.990         14.734         07:03:27:926         -20:52:19.78         101.1         N         Y           2463         0158         17.273         16.147         14.799         07:03:07.68         -20:46:17.21         118.8         Y           755         0162         17.273         16.123         14.836         07:03:01.582         -20:47:59.53         118.0         Y           556         0164         17.347         16.170         14.759         07:03:03.513         -20:46:47.57         122.6         591         125.1         Y           824         0165         17.364         16.169         14.776         07:03:03.513         -20:48:48.18         117.2         Y         Y           268         0177         17.379         16.243         14.876         07:03:07.204         -20:50:20.41         118.7         Y         Y           424         0179         17.411         16.243         14.897         07:03:02.643         -20:48:23.60         120.9         3763         120											1672	119.1	
2446         0142         17.132         15.990         14.734         07:03:27.926         -20:52:19.78         101.1         N           2450         0146         17:207         16.051         14.684         07:03:07.688         -20:45:48.97         119.5         Y           2463         0158         17:273         16.147         14.799         07:03:07.768         -20:46:17.21         118.8         Y           755         0162         17:273         16.123         14.836         07:03:07.588         -20:47:59.53         118.0         Y           556         0164         17.347         16.170         14.759         07:03:20.483         -20:46:47.57         122.6         591         125.1         Y           824         0165         17.364         16.169         14.776         07:03:07.204         -20:48:48.18         117.2         Y           268         0177         17.411         16.243         14.876         07:03:07.204         -20:50:20.41         118.7         Y           424         0179         17.411         16.235         15.099         07:02:52.319         -20:48:23.60         120.9         3763         120.1         Y           2474         0190 <td< td=""><td></td><td></td><td></td><td></td><td></td><td></td><td></td><td></td><td></td><td></td><td></td><td></td><td></td></td<>													
2450         0146         17.207         16.051         14.684         07:03:09:695         -20:45:48.97         119.5         Y           2463         0158         17:273         16.147         14.799         07:03:07:68         -20:46:17:21         118.8         Y           755         0162         17:273         16.123         14.836         07:03:01:582         -20:46:17:57         122.6         591         125.1         Y           556         0164         17:347         16.170         14:759         07:03:03:513         -20:46:47:57         122.6         591         125.1         Y           824         0165         17:364         16.169         14.776         07:03:03:513         -20:48:48.18         117.2         Y           268         0177         17:379         16.243         14.876         07:03:03:07:204         -20:50:20.41         118.7         Y           424         0179         17:411         16.243         14.876         07:03:03:04         -20:49:20.5         123.7         Y           1601         0182         17:404         16.256         14.928         07:03:03:06.082         -20:48:23.60         120.9         3763         120.1         Y											2343	104.0	
2463         0158         17.273         16.147         14.799         07:03:07.768         -20:46:17.21         118.8         Y           755         0162         17.273         16.123         14.836         07:03:01.582         -20:47:759.53         118.0         Y           556         0164         17.347         16.170         14.759         07:03:20.483         -20:46:47.57         122.6         591         125.1         Y           824         0165         17.364         16.169         14.776         07:03:03.513         -20:48:48.18         117.2         Y           268         0177         17.379         16.243         14.876         07:03:07.204         -20:50:20.41         118.7         Y           424         0179         17.411         16.248         07:03:02.643         -20:49:42.05         123.7         Y           1601         0182         17.404         16.256         14.928         07:03:02.643         -20:48:23.60         120.9         3763         120.1         Y           2474         0190         17.331         16.285         15.099         07:03:05.082         -20:48:57.53         121.2         Y           2477         0192         17.462 <t< td=""><td></td><td></td><td></td><td></td><td></td><td></td><td></td><td></td><td></td><td></td><td></td><td></td><td></td></t<>													
755         0162         17.273         16.123         14.836         07:03:01.582         -20:47:59.53         118.0         Y           556         0164         17.347         16.170         14.759         07:03:20.483         -20:46:47.57         122.6         591         125.1         Y           824         0165         17.364         16.169         14.776         07:03:03.513         -20:48:48.18         117.2         Y           268         0177         17.379         16.243         14.876         07:03:03.513         -20:48:48.18         117.2         Y           424         0179         17.411         16.243         14.887         07:03:13.240         -20:49:42.05         123.7         Y           1601         0182         17.404         16.256         14.928         07:03:05.082         -20:48:23.60         120.9         3763         120.1         Y           2474         0190         17.331         16.285         15.099         07:02:52.319         -20:44:38.17         80.6         N           2477         0192         17.462         16.301         14.911         07:02:53.302         -20:44:35.17         80.6         N           2477         0192         1													
556         0164         17.347         16.170         14.759         07:03:20.483         -20:46:47.57         122.6         591         125.1         Y           824         0165         17.364         16.169         14.776         07:03:07.204         -20:48:48.18         117.2         Y           268         0177         17.379         16.243         14.876         07:03:07.204         -20:50:20.41         118.7         Y           424         0179         17.411         16.243         14.897         07:03:13.240         -20:49:42.05         122.9         3763         120.1         Y           1601         0182         17.404         16.255         14.928         07:03:05.643         -20:48:23.60         120.9         3763         120.1         Y           2474         0190         17.331         16.285         15.099         07:02:52.319         -20:44:38.17         80.6         N         N           205         0191         17.463         16.301         14.911         07:02:53.302         -20:48:57.53         121.2         Y         Y           2477         0192         17.462         16.336         14.955         07:03:04.021         -20:49:07.82         121.5 <td< td=""><td></td><td></td><td></td><td></td><td></td><td></td><td></td><td></td><td></td><td></td><td></td><td></td><td></td></td<>													
824         0165         17.364         16.169         14.776         07:03:03.513         -20:48:48.18         117.2         Y           268         0177         17.379         16.243         14.876         07:03:07.204         -20:50:20.41         118.7         Y           424         0179         17.411         16.243         14.897         07:03:13.240         -20:49:20.05         123.7         Y           1601         0182         17.404         16.256         14.928         07:03:02.643         -20:48:23.60         120.9         3763         120.1         Y           2474         0190         17.331         16.285         15.099         07:02:52.319         -20:44:38.17         80.6         N           205         0191         17.463         16.301         14.911         07:03:05.082         -20:48:57.53         121.2         Y           2477         0192         17.462         16.301         14.911         07:02:53.302         -20:48:01.26         96.3         2185         96.3         N           246         0196         17.557         16.338         14.892         07:03:04.021         -20:49:07.82         121.5         3574         121.7         Y											591	125.1	
268         0177         17.379         16.243         14.876         07:03:07.204         -20:50:20.41         118.7         Y           424         0179         17.411         16.243         14.897         07:03:13.240         -20:49:42.05         123.7         Y           1601         0182         17.404         16.256         14.928         07:03:02.643         -20:48:23.60         120.9         3763         120.1         Y           2474         0190         17.331         16.285         15.099         07:03:05.082         -20:48:31.7         80.6         N           2477         0192         17.462         16.309         14.927         07:03:05.082         -20:48:57.53         121.2         Y           2477         0192         17.462         16.301         14.911         07:02:53.302         -20:48:01.26         96.3         2185         96.3         N           246         0196         17.557         16.338         14.892         07:03:06.471         -20:49:16.79         123.6         Y         121.7         Y           2489         0201         17.476         16.362         15.046         07:02:57.400         -20:52:58.15         57.6         N           197											371	123.1	
424         0179         17.411         16.243         14.897         07:03:13.240         -20:49:42.05         123.7         Y           1601         0182         17.404         16.256         14.928         07:03:02.643         -20:48:23.60         120.9         3763         120.1         Y           2474         0190         17.331         16.285         15.099         07:03:05.082         -20:44:38.17         80.6         N           205         0191         17.462         16.301         14.911         07:02:53.302         -20:48:57.53         121.2         Y           2477         0192         17.462         16.301         14.911         07:02:53.302         -20:48:01.26         96.3         2185         96.3         N           246         0196         17.557         16.338         14.892         07:03:06.471         -20:49:16.79         123.6         Y         Y           2489         0201         17.476         16.362         15.046         07:02:57.400         -20:52:58.15         57.6         N           1974         0207         17.582         16.402         14.944         07:03:19.393         -20:48:39.53         32.0         N           364         0215<													
1601         0182         17.404         16.256         14.928         07:03:02.643         -20:48:23.60         120.9         3763         120.1         Y           2474         0190         17:331         16.285         15.099         07:02:52.319         -20:44:38.17         80.6         N           205         0191         17:463         16.309         14.927         07:03:05.082         -20:48:57.53         121.2         Y           2477         0192         17:462         16.301         14.911         07:02:53.302         -20:48:01.26         96.3         2185         96.3         N           246         0196         17:557         16:338         14.892         07:03:06.471         -20:49:07.82         121.5         3574         121.7         Y           2489         0201         17:476         16:336         14.955         07:03:04.021         -20:49:07.82         121.5         3574         121.7         Y           1974         0207         17:582         16:402         14.944         07:03:19.393         -20:48:39.53         32.0         N           364         0215         17:641         16:488         15.085         07:03:09.19         -20:49:33.02         128.8													
205         0191         17.463         16.309         14.927         07:03:05.082         -20:48:57.53         121.2         Y           2477         0192         17.462         16.301         14.911         07:02:53:302         -20:48:01.26         96.3         2185         96.3         N           246         0196         17.557         16:338         14.892         07:03:06.471         -20:49:16.79         123.6         Y           164         0199         17.516         16:336         14.955         07:03:04.021         -20:49:07.82         121.5         3574         121.7         Y           2489         0201         17.476         16:362         15.046         07:02:57.400         -20:52:58.15         57.6         N         N           1974         0207         17:582         16:402         14.944         07:03:19.393         -20:48:39.53         32.0         N         N           364         0215         17:641         16:488         15.085         07:03:11.229         -20:49:33.02         128.8         N         N           2499         0217         17:491         16:539         15:129         07:03:03:48:855         -20:44:10.78         134.1         2822         1	1601		17.404	16.256	14.928	07:03:02.643	-20:48:23.60				3763	120.1	
2477         0192         17.462         16.301         14.911         07:02:53.302         -20:48:01.26         96.3         2185         96.3         N           246         0196         17.557         16.338         14.892         07:03:06.471         -20:49:16.79         123.6         Y           164         0199         17.516         16.336         14.955         07:03:04.021         -20:49:07.82         121.5         3574         121.7         Y           2489         0201         17.476         16.362         15.046         07:02:57.400         -20:52:58.15         57.6         N           1974         0207         17.582         16.402         14.944         07:03:19.393         -20:48:39.53         32.0         N           364         0215         17.641         16.488         15.085         07:03:11.229         -20:49:33.02         128.8         N           320         0217         17.491         16.559         15.299         07:03:09.119         -20:49:25.75         151.9         N           2507         0223         17.576         16.430         15.137         07:02:48.387         -20:44:10.78         134.1         2822         133.5         N	2474	0190	17.331	16.285	15.099	07:02:52.319	-20:44:38.17			80.6			
246       0196       17.557       16.338       14.892       07:03:06.471       -20:49:16.79       123.6       Y         164       0199       17.516       16.336       14.955       07:03:04.021       -20:49:07.82       121.5       3574       121.7       Y         2489       0201       17.476       16.362       15.046       07:02:57.400       -20:52:58.15       57.6       N         1974       0207       17.582       16.402       14.944       07:03:19.393       -20:48:39.53       32.0       N         364       0215       17.641       16.488       15.085       07:03:11.229       -20:49:33.02       128.8       N         320       0217       17.491       16.559       15.299       07:03:09.119       -20:49:25.75       151.9       N         2499       0219       17.570       16.430       15.137       07:02:48.855       -20:44:10.78       134.1       2822       133.5       N         2507       0223       17.576       16.497       15.274       07:02:48.387       -20:47:37.47       70.6       N         47       18.219       17.140       15.833       07:02:58.677       -20:50:56.07       1512       117.6       Y	205		17.463	16.309	14.927	07:03:05.082	-20:48:57.53			121.2			
164       0199       17.516       16.336       14.955       07:03:04.021       -20:49:07.82       121.5       3574       121.7       Y         2489       0201       17.476       16.362       15.046       07:02:57.400       -20:52:58.15       57.6       N         1974       0207       17.582       16.402       14.944       07:03:19.393       -20:48:39.53       32.0       N         364       0215       17.641       16.488       15.085       07:03:11.229       -20:49:33.02       128.8       N         320       0217       17.491       16.559       15.299       07:03:09.119       -20:49:25.75       151.9       N         2499       0219       17.570       16.430       15.137       07:02:48.855       -20:44:10.78       134.1       2822       133.5       N         2507       0223       17.576       16.497       15.274       07:02:48.387       -20:47:37.47       70.6       N         2522       0231       17.802       16.584       15.147       07:03:28.589       -20:46:26.35       122.1       Y         47       18.219       17.140       15.833       07:02:58.677       -20:50:56.07       1512       117.6       Y											2185	96.3	
2489         0201         17.476         16.362         15.046         07:02:57.400         -20:52:58.15         57.6         N           1974         0207         17.582         16.402         14.944         07:03:19.393         -20:48:39.53         32.0         N           364         0215         17.641         16.488         15.085         07:03:11.229         -20:49:33.02         128.8         N           320         0217         17.491         16.559         15.299         07:03:09.119         -20:49:25.75         151.9         N           2499         0219         17.570         16.430         15.137         07:02:48.855         -20:44:10.78         134.1         2822         133.5         N           2507         0223         17.576         16.497         15.274         07:02:48.387         -20:47:37.47         70.6         N           2522         0231         17.802         16.584         15.147         07:03:28.589         -20:46:26.35         122.1         Y           47         18.219         17.140         15.833         07:02:58.677         -20:50:56.07         1512         117.6         Y           693         17.215         15.974         14.572													
1974         0207         17.582         16.402         14.944         07:03:19.393         -20:48:39.53         32.0         N           364         0215         17.641         16.488         15.085         07:03:11.229         -20:49:33.02         128.8         N           320         0217         17.491         16.559         15.299         07:03:09.119         -20:49:25.75         151.9         N           2499         0219         17.570         16.430         15.137         07:02:48.855         -20:44:10.78         134.1         2822         133.5         N           2507         0223         17.576         16.497         15.274         07:02:48.387         -20:47:37.47         70.6         N           2522         0231         17.802         16.584         15.147         07:03:28.589         -20:46:26.35         122.1         Y           47         18.219         17.140         15.833         07:02:58.677         -20:50:56.07         1512         117.6         Y           693         17.215         15.974         14.572         07:02:59.738         -20:49:33.36         1827         120.9         Y           343         17.204         16.062         14.759											3574	121.7	
364         0215         17.641         16.488         15.085         07:03:11.229         -20:49:33.02         128.8         N           320         0217         17.491         16.559         15.299         07:03:09.119         -20:49:25.75         151.9         N           2499         0219         17.570         16.430         15.137         07:02:48.855         -20:44:10.78         134.1         2822         133.5         N           2507         0223         17.576         16.497         15.274         07:02:48.387         -20:47:37.47         70.6         N           2522         0231         17.802         16.584         15.147         07:03:28.589         -20:46:26.35         122.1         Y           47         18.219         17.140         15.833         07:02:58.677         -20:50:56.07         1512         117.6         Y           693         17.215         15.974         14.572         07:02:59.738         -20:49:33.36         1827         120.9         Y           343         17.204         16.062         14.759         07:03:10.339         -20:47:59.24         2184         119.8         Y           2465         17.355         16.188         14.831													
320         0217         17.491         16.559         15.299         07:03:09.119         -20:49:25.75         151.9         N           2499         0219         17.570         16.430         15.137         07:02:48.855         -20:44:10.78         134.1         2822         133.5         N           2507         0223         17.576         16.497         15.274         07:02:48.387         -20:47:37.47         70.6         N           2522         0231         17.802         16.584         15.147         07:03:28.589         -20:46:26.35         122.1         Y           47         18.219         17.140         15.833         07:02:58.677         -20:50:56.07         1512         117.6         Y           693         17.215         15.974         14.572         07:02:59.738         -20:49:33.36         1827         120.9         Y           343         17.204         16.062         14.759         07:03:10.339         -20:47:59.24         2184         119.8         Y           2465         17.355         16.188         14.831         07:03:27.495         -20:51:15.08         236         121.0         Y           2469         17.419         16.244         14.997													
2499       0219       17.570       16.430       15.137       07:02:48.855       -20:44:10.78       134.1       2822       133.5       N         2507       0223       17.576       16.497       15.274       07:02:48.387       -20:47:37.47       70.6       N         2522       0231       17.802       16.584       15.147       07:03:28.589       -20:46:26.35       122.1       Y         47       18.219       17.140       15.833       07:02:58.677       -20:50:56.07       1512       117.6       Y         693       17.215       15.974       14.572       07:02:59.738       -20:49:33.36       1827       120.9       Y         343       17.204       16.062       14.759       07:03:10.339       -20:47:59.24       2184       119.8       Y         2465       17.355       16.188       14.831       07:03:27.495       -20:51:15.08       236       121.0       Y         2469       17.419       16.244       14.997       07:02:58.142       -20:44:02.69       2846       122.9       Y													
2507       0223       17.576       16.497       15.274       07:02:48.387       -20:47:37.47       70.6       N         2522       0231       17.802       16.584       15.147       07:03:28.589       -20:46:26.35       122.1       Y         47       18.219       17.140       15.833       07:02:58.677       -20:50:56.07       1512       117.6       Y         693       17.215       15.974       14.572       07:02:59.738       -20:49:33.36       1827       120.9       Y         343       17.204       16.062       14.759       07:03:10.339       -20:47:59.24       2184       119.8       Y         2465       17.355       16.188       14.831       07:03:27.495       -20:51:15.08       236       121.0       Y         2469       17.419       16.244       14.997       07:02:58.142       -20:44:02.69       2846       122.9       Y											2822	133.5	
2522       0231       17.802       16.584       15.147       07:03:28.589       -20:46:26.35       122.1       Y         47       18.219       17.140       15.833       07:02:58.677       -20:50:56.07       1512       117.6       Y         693       17.215       15.974       14.572       07:02:59.738       -20:49:33.36       1827       120.9       Y         343       17.204       16.062       14.759       07:03:10.339       -20:47:59.24       2184       119.8       Y         2465       17.355       16.188       14.831       07:03:27.495       -20:51:15.08       236       121.0       Y         2469       17.419       16.244       14.997       07:02:58.142       -20:44:02.69       2846       122.9       Y											2022	1.0.0	
47       18.219       17.140       15.833       07:02:58.677       -20:50:56.07       1512       117.6       Y         693       17.215       15.974       14.572       07:02:59.738       -20:49:33.36       1827       120.9       Y         343       17.204       16.062       14.759       07:03:10.339       -20:47:59.24       2184       119.8       Y         2465       17.355       16.188       14.831       07:03:27.495       -20:51:15.08       236       121.0       Y         2469       17.419       16.244       14.997       07:02:58.142       -20:44:02.69       2846       122.9       Y													
693     17.215     15.974     14.572     07:02:59.738     -20:49:33.36     1827     120.9     Y       343     17.204     16.062     14.759     07:03:10.339     -20:47:59.24     2184     119.8     Y       2465     17.355     16.188     14.831     07:03:27.495     -20:51:15.08     236     121.0     Y       2469     17.419     16.244     14.997     07:02:58.142     -20:44:02.69     2846     122.9     Y											1512	117.6	
343       17.204       16.062       14.759       07:03:10.339       -20:47:59.24       2184       119.8       Y         2465       17.355       16.188       14.831       07:03:27.495       -20:51:15.08       236       121.0       Y         2469       17.419       16.244       14.997       07:02:58.142       -20:44:02.69       2846       122.9       Y													
2469 17.419 16.244 14.997 07:02:58.142 -20:44:02.69 2846 122.9 Y													
	2465			16.188		07:03:27.495	-20:51:15.08				236	121.0	Y
1200 17.040 16.710 15.262 07.02.04.617 20.40.12.06 2026 120.0 37	2469		17.419	16.244	14.997		-20:44:02.69				2846	122.9	
1396 17.849 10.710 13.303 07:05:04.017 -20:48:12.86 3836 120.9 N	1398		17.849	16.710	15.363	07:03:04.617	-20:48:12.86				3836	120.9	N

Table 3. (continuation)

ID	$ID_{\mathrm{WEBDA}}$	В	V	Ι	RA (2000) hh:mm:ss	Dec (2000) dd:pp:ss	$\begin{array}{c} \rm RV_1 \\ \rm km~s^{-1} \end{array}$	$\begin{array}{c} \rm RV_2 \\ \rm km~s^{-1} \end{array}$	$ m RV_3$ $ m km~s^{-1}$	$ID_4$	$ m RV_4$ $ m km~s^{-1}$	Member?
215		17.966	16.992	15.777	07:03:05.211	-20:52:45.36				153	61.1	N
2394		16.754	15.441	13.946	07:02:41.994	-20:50:51.89				1530	98.9	N
2421		16.990	15.781	14.444	07:03:33.150	-20:50:30.41				1573	59.8	N
2289		16.234	14.748	13.105	07:02:59.724	-20:49:49.49				1755	126.9	N
2404		17.059	15.583	14.018	07:03:34.302	-20:46:52.81				2403	64.8	N
1435		18.156	17.139	16.045	07:03:09.446	-20:51:01.66				250	87.2	N
2677		18.330	17.373	16.301	07:03:26.870	-20:46:16.91				2510	18.3	N
2425		17.068	15.819	14.457	07:03:32.502	-20:50:48.01				266	130.9	N
2609		18.011	17.022	15.888	07:03:20.741	-20:44:06.15				2827	38.5	N
2396		16.715	15.480	14.153	07:02:42.796	-20:43:33.07				2911	109.1	N
2422		16.940	15.791	14.527	07:02:58.306	-20:43:04.78				2975	105.6	N
73		18.148	16.987	15.667	07:03:00.315	-20:46:42.59				3332	130.6	N
185		17.107	15.860	14.448	07:03:04.458	-20:49:18.20				3562	51.3	N
745		17.175	16.041	14.696	07:03:01.333	-20:49:26.93				390	114.9	N
2459		17.249	16.132	14.785	07:03:23.382	-20:46:49.24				589	135.0	N
2418		16.917	15.736	14.396	07:03:33.972	-20:46:00.33				650	107.2	N
2437		17.135	15.922	14.638	07:02:42.171	-20:46:05.23				651	121.7	Y

relatively metal-rich and cool (i.e., with very crowded spectra) stars as the RGB ones in To 2.

Whether CMa, and perhaps the Monoceros ring, are truly of extragalactic origin, or are instead due to disc warping and flaring, or spiral arms, or a combination of these phenomena, and whether To 2 is truly associated to these structures, or is "simply" a normal, Galactic-disc open cluster, the study of this part of the Galactic disc is important. Further observations, both photometric and spectroscopic, are then welcome, in particular to settle the question of the possible chemical inhomogeneity,

#### 3 OUR DATA

The three clusters were observed from two observatories and with three telescopes; a log of the observations is given in Table 4. The final photometric catalogues will be made available at the WEBDA. They will present the  $(B)VI_C$  magnitudes with errors, pixel coordinates, and equatorial coordinates (tied to the GSC2 Catalogue using CataPack, a software written by P. Montegriffo at the Bologna Observatory).

#### 3.1 Be 20 and Be 66

Observations of the two clusters and the two control fields were obtained at the Telescopio Nazionale Galileo (TNG) on Canary Islands, during two nights in October and November 2000. We used DOLORES (Device Optimized for LOw RESolution), characterized by a field of view of  $9.4 \times 9.4$  arcmin² and a scale of 0.275''/pixel. Since in these two runs we also observed Be 17 (Bragaglia et al. 2006a) and NGC 6939 (Andreuzzi et al. 2004), we refer to those publications for details on observation and reduction procedures. Very briefly, we used the package DAOPHOT-II (Stetson 1987; Davis 1994) to obtain PSF magnitudes, we corrected them to the same scale of aperture photometry and calibrated to the standard Johnson-Cousins system using Landolt's areas (Landolt 1992). The calibration equations adopted for Be 20 and its control field observed on the same night, are:

$$V = v - 0.0947 \times (v - i) + 1.1917 \ (rms = 0.014)$$

$$I_C = i - 0.0060 \times (v - i) + 0.7638 \ (rms = 0.025)$$

The calibration equations adopted for Be 66 are:

$$B = b + 0.0475 \times (b - v) + 1.4211 \ (rms = 0.012)$$

$$V = v - 0.0959 \times (v - i) + 1.2003 \ (rms = 0.012)$$

$$I_C = i + 0.0422 \times (v - i) + 0.7248 \ (rms = 0.012)$$

The calibration equations adopted for the control field of Be 66 are:

$$B = b + 0.0421 \times (b - v) + 1.4043 \ (rms = 0.012)$$

$$V = v - 0.0947 \times (v - i) + 1.1917 \ (rms = 0.014)$$

$$I_C = i + 0.0017 \times (v - i) + 0.7589 \ (rms = 0.024),$$

where b,v, and i, are the aperture corrected instrumental magnitudes after correction also for extinction and exposure time, and B,V, and  $I_C$  are the output magnitudes, calibrated to the Johnson-Cousins standard system.

Finally, the completeness level of our photometry was derived with extensive artificial stars experiments, as in previous papers of this project. The completeness factors are shown in Table 5. From these experiments we also derived the errors typically associated to each magnitude level, that are used in Sect. 5 to build the synthetic CMDs.

We compared our photometry for Be 20 with the ones of the two papers presenting the derivation of cluster parameters and readily available through the WEBDA, i.e., to the MacMinn et al. (1994) and the Durgapal et al. (2001) data.

We counter-identified stars in the different catalogues and the results are presented in Fig. 1. In particular panels (a) and (b) in the figure show the comparison to the MacMinn et al. (1994) data, while panels (c) and (d) show the comparison to the Durgapal et al. (2001) data. For each star in common between the three catalogs, V and I are the magnitudes in our photometry calibrated with the equations given in the text;  $V_M$  and  $I_M$  are the corresponding magnitudes in the catalog of MacMinn et al. (1994) while  $V_D$  and  $I_D$  are the magnitudes of the corresponding stars in the catalog of Durgapal et al. (2001).

Table 4. Log of observations for the clusters and the control fields

Field	$\alpha_{2000}$	$\delta_{2000}$	UT Date (dd/mm/yy)	exptime B (s)	exptime V (s)	exptime I (s)	Telescope	Istrument
Be 20 Be 20 - control	$05^h 32^m 34^s 05^h 32^m 34^s$		24/11/2000 24/11/2000	_ _	900, 120, 20 600, 120, 20	900, 120, 20 480, 120, 20	TNG TNG	DOLORES DOLORES
Be 66 Be 66 - control	$03^h 04^m 06^s \\ 03^h 04^m 20^s$		03/10/2000 24/11/2000	1300, 600, 300, 60 1800, 240, 30	2×900, 60, 10 900, 120, 20	900, 60, 10 120, 20	TNG TNG	DOLORES DOLORES
To 2 To 2 - control	$07^{h}02^{m}57^{s}$ $07^{h}06^{m}06^{s}$	-20°49′ 53″ -20°50′ 20″	07-08/03/1995 15/05/2001 15/01/2002 15-16/05/2001	1500, 300 200, 2×10 1800	2×720, 300, 2×60 150, 10 1200 600, 60, 10	2×720, 243, 60 120, 10 2×900 500, 60, 10	Danish Danish NTT Danish	Direct camera DFOSC SuSI2 DFOSC

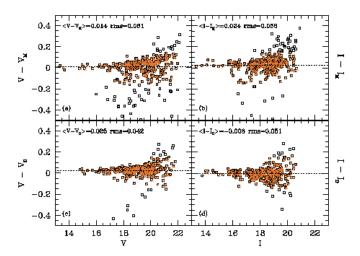
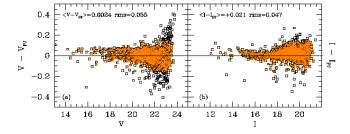


Figure 1. Comparison between our photometry and literature data for Be 20. Panels (a) and (b) show the comparison to the MacMinn et al. (1994) data; panels (c) and (d) show the comparison to the Durgapal et al. (2001)



**Figure 2.** Comparison between our photometry and the one by Phelps & Janes (1996) for Be 66.

For Be 66, the comparison was done to Phelps & Janes (1996), again only in the V and I filters, since they did not obtain B photometry. The results are shown in Fig. 2. For each star in common between the two catalogs, V and I are the magnitudes in our photometry calibrated with the equations given in the text.  $V_{PJ}$  and  $I_{PJ}$  are the corresponding magnitudes in the catalog of Phelps & Janes (1996).

For both clusters, the differences between the different photometries have been computed retaining only well counteridentified stars (corresponding to the subsamples indicated in colour in the electronic version of the figures), with a difference in magnitude less than 0.15 mag, in absolute value. Differences are of the order of 0.02-0.03 mag in all cases.

#### 3.2 To 2

Observations were obtained in La Silla, Chile, using two telescopes and three different instruments: a direct CCD camera (6.4×6.4 arcmin<sup>2</sup>) in 1995 and DFOSC (Danish Faint Object Spectrograph and Camera, 13×13 arcmin<sup>2</sup>) in 2001, both mounted at the Danish telescope, and SuSI2 (Super Seeing Imager 2,  $5 \times 5$  arcmin<sup>2</sup>), mounted at the New Tecnology Telescope (NTT) in 2002. We observed a field centred on the cluster and one about 50 arcmin away as a comparison to separate cluster and field stars.

The data reduction followed a standard procedure, see for instance Di Fabrizio et al. (2005). Unfortunately, none of the nights turned out to be truly photometric, as we found out by comparison to the published photometries by Kubiak et al. (1992) and Phelps et al. (1994). We decided to calibrate our photometry to the one by Kubiak et al., since it was the deepest one. No similar solution has been possible for the comparison field; however, the photometric accuracy obtained for it is enough for our goals (we only wish to separate cluster and field stars), also because we only have quite short exposures for this field.

The results for the completeness tests are shown in Table 5. The final catalogue for To 2 contains 6073 stars. The limiting magnitude depends on the distance from the centre, since we obtained only short exposures with the widest field. In the following we will consider only the central  $5\times5$  arcmin<sup>2</sup> region, observed with SuSI2 on NTT, to derive the cluster properties.

# THE COLOUR - MAGNITUDE DIAGRAMS

• Be 20 - Fig. 3 shows the CMD obtained for the field centred on Be 20 (left panel) and for the control field (right panel); the mid-

**Table 5.** Completeness level for the clusters and control fields of Be 20 and Be 66 and for the central field of To 2 as measured from the SuSI2 observations; mag is the calibrated magnitude  $(B, V, \text{ or } I_C)$ .

mag	$c_V$ Be	c <sub>I</sub> 20	c <sub>V</sub> Be 20-	c <sub>I</sub> control	$c_B$	c <sub>V</sub> Be 66	$c_I$	с <sub>В</sub> Ве	c <sub>V</sub> : 66-con	c <sub>I</sub> crol	$c_B$	с <sub>V</sub> То 2	$c_I$
15.5	1.00	1.00	1.00	1.00	1.00	1.00	1.00	1.00	1.00	1.00	1.00	1.00	1.00
16.0	1.00	0.96	0.98	0.99	1.00	1.00	1.00	1.00	1.00	0.99	1.00	1.00	1.00
16.5	0.98	0.93	0.98	0.96	1.00	1.00	1.00	1.00	1.00	0.99	1.00	1.00	1.00
17.0	0.94	0.91	0.97	0.96	1.00	1.00	1.00	1.00	1.00	0.97	1.00	1.00	1.00
17.5	0.94	0.88	0.95	0.94	1.00	1.00	1.00	1.00	0.99	0.97	1.00	1.00	1.00
18.0	0.92	0.85	0.91	0.98	1.00	1.00	1.00	1.00	0.98	0.95	1.00	1.00	1.00
18.5	0.91	0.77	0.91	0.93	1.00	0.96	0.94	1.00	0.98	0.94	1.00	1.00	1.00
19.0	0.91	0.67	0.90	0.88	1.00	0.97	0.92	0.99	0.95	0.93	1.00	1.00	1.00
19.5	0.88	0.47	0.86	0.76	0.99	0.96	0.89	0.99	0.98	0.85	1.00	1.00	1.00
20.0	0.79	0.27	0.75	0.53	0.97	0.96	0.83	0.96	0.92	0.60	1.00	1.00	1.00
20.5	0.68	0.08	0.55	0.30	0.96	0.95	0.78	0.94	0.86	0.32	1.00	1.00	0.97
21.0	0.46	0.00	0.31	0.10	0.97	0.94	0.67	0.92	0.85	0.13	1.00	1.00	0.82
21.5	0.23	0.00	0.13	0.00	0.95	0.93	0.43	0.92	0.71	0.03	1.00	1.00	0.80
22.0	0.10	0.00	0.03	0.00	0.92	0.86	0.19	0.90	0.48	0.00	0.93	1.00	0.75
22.5	0.02	0.00	0.01	0.00	0.92	0.69	0.00	0.80	0.24	0.00	0.85	0.95	0.68
23.0	0.01	0.00	0.00	0.00	0.80	0.38	0.00	0.56	0.11	0.00	0.81	0.85	0.38
23.5	0.00	0.00	0.00	0.00	0.50	0.03	0.00	0.30	0.02	0.00	0.79	0.77	0.14
24.0	0.00	0.00	0.00	0.00	0.16	0.00	0.00	0.15	0.00	0.00	0.76	0.77	0.10
24.5	0.00	0.00	0.00	0.00	0.00	0.00	0.00	0.04	0.00	0.00	0.70	0.68	0.03
25.0	0.00	0.00	0.00	0.00	0.00	0.00	0.00	0.00	0.00	0.00	0.65	0.50	0.00
25.5	0.00	0.00	0.00	0.00	0.00	0.00	0.00	0.00	0.00	0.00	0.39	0.39	0.00
26.0	0.00	0.00	0.00	0.00	0.00	0.00	0.00	0.00	0.00	0.00	0.16	0.20	0.00
26.5	0.00	0.00	0.00	0.00	0.00	0.00	0.00	0.00	0.00	0.00	0.03	0.03	0.00
27.0	0.00	0.00	0.00	0.00	0.00	0.00	0.00	0.00	0.00	0.00	0.00	0.00	0.00

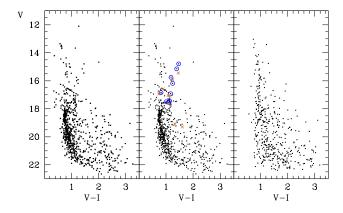


**Figure 3.** CMDs for Be 20 (left panel) and the control field (right panel). In the middle panel we indicate with different symbols member (blue open circles) and non member (orange crosses) stars, according to their RVs. The latter are listed in Table 1, together with the references.

dle panel indicates (with larger symbols) the stars for which information on membership is available thanks to the RVs. We clearly see the main sequence for about 4 magnitudes below the MSTO, located around  $V=18.2,\,V-I=0.7.$  We also identify the red clump with the few stars at  $V\simeq 16.0,\,V-I\simeq 1.2.$  Given the field stars distribution, stars above the MSTO may be attributed to a blue stragglers population or to fore/background contamination. Indeed, of the three stars with measured RV present in this region, two are field objects and one is a cluster member. More could be said only after decontamination, either statistical or (better) through actual measurement of the individual membership status via RV or proper motion.

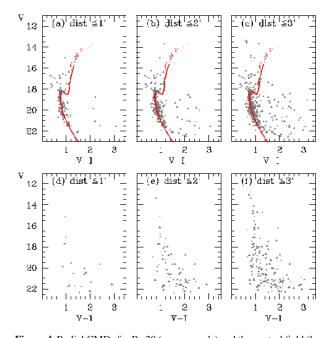


**Figure 4.** Radial CMDs for Be 20 (upper panels) and the control field (lower panels). The stars within the 1', 2', 3' radii are 136, 269, 401 for the cluster and 19, 70, 153 for the control field, respectively. In the upper panels we show one of the best-fitting solutions (see Sect. 5.1) to guide the eye.

Fig. 4 shows the radial distribution of stars in the cluster field, compared to an equal area in the control field; this is very useful

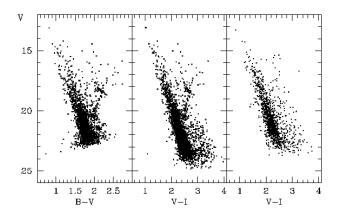
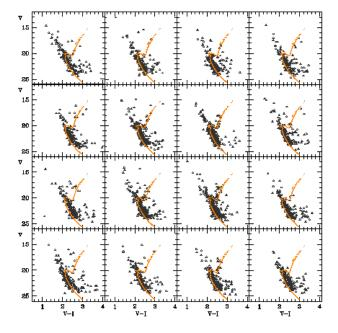


Figure 5. CMDs for Be 66 (left and middle panels) and the control field (right panel, shown only in the V, V-I plane).



**Figure 6.** CMDs obtained in different regions  $(500 \times 500 \text{ pixels wide, i.e.}, 2.2 \times 2.2 \text{ arcmin}^2)$  of Be 66. East is to the left and North to the top, and the cluster is located at the centre of the field of view. The isochrone (FST models with age 3 Gyr and metallicity Z=0.006) shown here represents one of the best solutions (see Sect. 5) and clearly indicates that differential reddening is present, but only at a few per cent level.

to better understand which are the true cluster sequences and the degree of field contamination (see also next Sect.).

• Be 66 - The CMDs for Be 66 and the control field are presented in Fig. 5. Notice the very red colours of the sequences, due to the high reddening, and the width of the evolutionary sequences. Janes & Phelps (1994) suspected the presence of differential reddening, a very reasonable possibility given its high value. We estimate that a variation of only a few per cent (see Sect.5.2) is sufficient to justify the observed spread. Fig. 6 shows a graphical representation of this: the CMDs obtained in sub-regions of the frame are all similar to each other and can be fit by the same isochrone (see Sect. 5.2 for the choice of the best one) once some difference in reddening is accepted. We notice in particular that the reddest CMDs correspond to the most eastern subregions in the two central rows of Fig. 6; while the least reddened CMDs are sparsely located: one in the bottom-left (south-east) panel and the other in the third top panel from left (north-east). This distribution suggests a clumpy/inhomogeneous extinction, rather than a systematic reddening variation.

In spite of the high dispersion and contamination, the main evolutionary phases, MS, MSTO, SGB, RGB, clump and possibly AGB are quite well defined, with the MSTO at  $V\simeq 20.1$ ,  $B-V\simeq 1.6$ , and  $V-I\simeq 2.1$ , and the clump - RGB intersection at  $V\simeq 18.4$ ,  $B-V\simeq 2.2$ , and  $V-I\simeq 2.7$ .

• To 2 – The situation for To 2 is more complicated, since the cluster was observed with three different instruments with very different field of view, and to very different depths (see Table 4). Fig. 7 shows the combination of all data for the central field in the upper row, left and middle panels, for the V, B-V and V, V-I CMDs, respectively. The entire control field is shown in the upper, right panel, only in V, V-I; we can immediately appreciate the different depths reached by the various instruments.

To better separate the cluster CMD from the background, we plot in the lower panel of Fig. 7 only stars within a 2 arcmin distance from the cluster centre (left and middle panels) and within the same area in the control field (right panel). The evolutionary phases are much better recognizable, with the MSTO at  $V \simeq 17.5$ ,  $B-V \simeq 0.60$ , and  $V-I \simeq 0.65$ , and the red clump at  $V \simeq 16.2$ ,  $B-V \simeq 1.12$ , and  $V-I \simeq 1.33$ .

Member and non member stars, according to their RVs (see Table 3), are indicated with different symbols in the V,B-V CMD. This information is very useful to confirm the position of the RGB and red clump; unfortunately, RVs are not available for stars on the MS and the MSTO. However, as found by Frinchaboy et al. (2008, see their Sects. 3 and 6), even if the difference in RV between the cluster and the Galactic field stars is large enough to ensure a good decontamination, the same is not valid for the GASS/Monoceros component and some confusion may still be present.

If we further restrict to the stars within 1 arcmin from the cluster centre, where the cluster stars dominate over the background, it is possible to see a clear indication of the presence of binaries, as shown in Fig. 8(a). The secondary MS is visible above and to the red of the single-stars MS; we use here B-I to have a larger baseline in colour. In Fig. 8(b) we indicate the two MSs; it is evident how the secondary, binary sequence complicates the definition of the position of the single-stars MSTO.

The difference in magnitute between the MSTO and the red clump ( $\delta V$ ) can be used as an age indicator, after a suitable calibration (e.g., Phelps & Janes 1996; Friel 1995; Bragaglia & Tosi 2006). This may be useful especially when dealing with large samples and/or a photometry that does not reach much below

**Table 6.** Values for  $\delta V$ , age in Gyr, Z, and [Fe/H] from high-resolution spectroscopy for the seven clusters analysed after Bragaglia & Tosi (2006). See text for the references.

Cluster	$\delta V$	age	Z	[Fe/H]	References
Be 17	2.9	8.5	0.008	-0.10	1, 2
Be 32	2.6	5.2	0.008	-0.29	3, 4
Be 20	2.2	5.8	0.008	-0.30	5, 4
King 11	2.2	4.5	0.02	-	3, -
Be 66	1.7	3.8	0.008	-0.48	5, 6
To 2	1.3	1.7	0.008	-0.31	5, 7
NGC 3960	0.8	0.9	0.02	-0.12	8, 8

the MSTO. In Table 6 we indicate these values (measured as described in Bragaglia & Tosi 2006) for both the three OCs analysed here and four others we published after Bragaglia & Tosi (2006). We also give other relevant information, like age and metallicity (obtained with the synthetic CMD technique and the BBC tracks, see Sect. 5) and [Fe/H]. The last column gives references for the parameters derived from photometry (Cols. 2-4, all by our group) and from high-resolution spectroscopy (Col. 5), respectively. The references are: 1: Bragaglia et al. (2006a); 2: Friel, Jacobson, & Pilachowski (2005); 3: Tosi et al. (2007); 4: Sestito et al. (2008); 5: this paper; 6: Villanova et al. (2005); 7: Villanova et al. (2010); 8: Bragaglia et al. (2006b). In Fig. 9 we plot the values of  $\delta V$  versus age derived using stellar models for all OCs in the BOCCE sample. The relation is clearly not a simple one, as witnessed by the spread, only a part of which is due to errors. Metallicity plays surely a role, see e.g., Twarog & Anthony-Twarog (1989) who decided to use a different indicator, combining differences in magnitude and colour, to take it into account. We do not derive here a relation between  $\delta V$  and age, deferring the task to when more OCs will be available on our scale.

#### 5 CLUSTER PARAMETERS

As for all the clusters of the BOCCE project (see Bragaglia & Tosi 2006 and references therein), we have derived age, distance and reddening following the synthetic CMD method originally described by Tosi et al. (1991). The best values of the parameters are found by selecting the cases providing synthetic CMDs with morphology, colours, number of stars in the various evolutionary phases and luminosity functions (LFs) in better agreement with the observational ones. To evaluate the goodness of the model predictions we quantitatively compare them with the observational LFs, stellar magnitude and colour distributions, and number of objects at the MSTO, the clump and the RGB. As discussed by Kalirai & Tosi (2004) and Tosi et al. (2007), where the luminosity and colour distributions of each model were independently compared with the data using a Kolmogorov-Smirnov test and a  $\chi^2$  test, even sophisticated statistical procedures do not provide safer estimates of the cluster parameters. This is due to the background/foreground contamination and to the small number of objects usually measured in key evolutionary phases, such as the MSTO, the red clump and the SGB, fundamental in the identification of the cluster age. In the most favorable cases, the statistical tests confirm our choices of best synthetic models. In the cases of the three systems presented here, the parameter selection is even more uncertain, due to further decontamination problems related to the complicated and inhomogeneous distribution of their fore/background interlopers. Yet, in

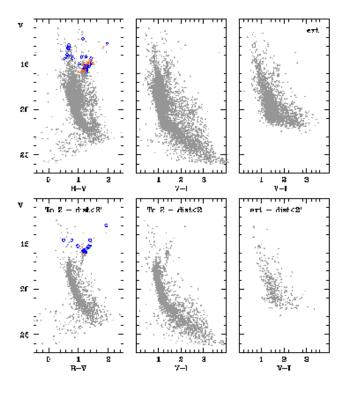


**Figure 7.** V, B-V and V, V-I CMDs for To 2 and the comparison field. The upper panels show the entire field, while the lower panels show only stars within a 2 arcmin distance. We also indicate, only for the V, B-V diagram, member (blue open circles) and non member (orange crosses) stars, according to their RVs (see Table 3).

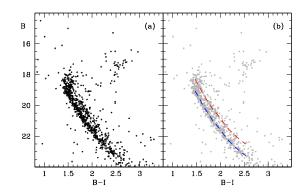


**Figure 8.** (a) CMD in B,B-I of the central region of To 2 (within a radius of 1 arcmin) showing the binary sequence. (b) The same, but showing the MS ridge line and the same line shifted by 0.7 mag brighter.

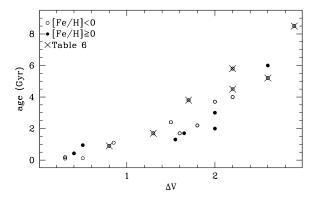


**Figure 9.**  $\delta V$  versus age for the 23 OCs presently available in the BOCCE sample, 16 clusters from Bragaglia & Tosi (2006), seven from Table 6. The meaning of the different symbols is indicated in the figure.

these unfavourable conditions the synthetic CMD approach is even safer (or less unsafe) than isochrone fitting than in standard cases, thanks to its capability to exploit all the available information on shape, population and position in the CMD of the various evolutionary phases. The method cannot provide strictly unique results, but allows to significantly reduce the range of acceptable parameters.

In our procedure, the synthetic stars, extracted from the adopted stellar evolutionary tracks with a Monte Carlo approach taking into accout the adopted initial mass function (IMF) and star formation law, are attributed the photometric error derived from the artificial stars tests performed on the actual images. For all the BOCCE clusters we assume a Salpeter's IMF and a constant star formation lasting 5 Myr from the epoch of activation. The extracted stars are retained in (or excluded from) the synthetic CMD according to the photometry completeness factors listed in Table 5. We have computed the synthetic CMDs both with and without taking into account the possible contribution from unresolved binaries (see Bragaglia & Tosi 2006 for a description of how binaries are included in the synthetic CMDs). Binary members are assumed to follow the same initial mass function (Salpeter's) as isolated stars and to have random mass ratio between primary and secondary components. In no case were the CMDs without binaries in agreement with the obervational ones. All the CMDs discussed here assume that 30% of the cluster measured stars are actually unresolved binaries. This fraction is consistent with what we find for the majority of the BOCCE clusters.

As usual, to test the effects of the adopted stellar evolution models on the derived parameters, we run the simulations with three different types of stellar tracks, with different assumptions for the treatment of convection, opacities and equation of state. The adopted models are listed in Table 7, where the corresponding references are also given, as well as the model metallicity and the information on their corresponding overshooting assumptions.

To estimate the metallicity which better reproduces the photometric properties of the cluster, we have created the synthetic CMDs adopting, for each type of stellar models, metallicities ranging from solar down to Z=0.004. We still assume as solar metallicity models those with Z=0.02, both for consistency with the BOCCE previous studies (see Bragaglia & Tosi 2006) and because they are the ones calibrated on the Sun by their authors. We consider only as indicative the metallicities obtained with our photo-

**Table 7.** Stellar evolution models adopted for the synthetic CMDs. The FST models actually adopted here are an updated version of the published ones (Ventura, private communication).

Set	metallicity	overshooting	Reference
BBC	0.008	yes	Fagotto et al. 1994
BBC	0.004	yes	Fagotto et al. 1994
BBC	0.02	yes	Bressan et al. 1993
FRA	0.006	no	Dominguez et al. 1999
FRA	0.01	no	Dominguez et al. 1999
FRA	0.02	no	Dominguez et al. 1999
FST	0.006	$\eta$ =0.00,0.02,0,03	Ventura et al. 1998
FST	0.01	$\eta$ =0.00,0.02,0,03	Ventura et al. 1998
FST	0.02	$\eta$ =0.00,0.02,0,03	Ventura et al. 1998

metric studies and refer to high resolution spectroscopy for a safer determination of the chemical abundances.

The transformations from the theoretical luminosity and effective temperature to the Johnson-Cousins magnitudes and colours have been performed using the Bessell, Castelli & Pletz (1998 and private communication) conversion tables of the metallicity of the adopted models. We assume  $A_V = (3.25 + 0.25 \times (B - V) + 0.05 \times E(B-V)) \times E(B-V)$  and  $E(V-I) = 1.25 \times E(B-V) \times [1 + 0.06(B-V)_0 + 0.014E(B-V)]$  from Dean et al. (1978) for all sets of models. Using the same source for the conversion tables for all models, we can be confident that the differences in the synthetic CMDs (and therefore in the cluster parameters) resulting from different stellar models must be fully ascribed to the intrinsic differences (input physics, opacities, etc.) of the models themselves and not to different photometric conversions.

## 5.1 Be 20

To minimize contamination without losing too many stars, we considered as reference CMD the diagram of the stars located within 2' from the cluster centre. As shown in Fig. 4, this is the region better compromising the two needs of removing contamination and having enough objects to define the key evolutionary phases. The CMD of this central circle is shown in the top panel of Fig. 10. It contains 269 stars, with 9 secure members (from the RV) nicely defining the red clump and the RGB, as shown in the central panel of Fig. 3. Since the control field of the same area contains 70 stars, we assumed that the cluster members within 2' are 200 and created the synthetic CMDs with this number of objects.

Fig. 10 shows the synthetic CMDs in better agreement with the data for each set of tracks, selected by minimizing the differences between morphology, star counts, luminosity and colour functions in the observational and synthetic MS, MSTO, SGB, RGB and clump phases. The top panel of the Figure shows the reference CMD, the panels in the central row show the best synthetic V, V - I CMDs obtained with the BBC, FRA, and FST models, overimposed to the CMD of the control field stars. The V, B - V synthetic CMDs corresponding to the same cases are shown in the bottom panels.

As apparent from Fig. 4, field contamination affects mostly the CMD portion fainter than  $V \simeq 18$ , but interlopers are present also at brighter magnitudes. Moreover, from that Figure and from the comparison of the top panel with the central row panels of Fig. 10, the CMD of the control field stars turns out to be not quite the same as that of the cluster field contaminants. This circumstance, as well

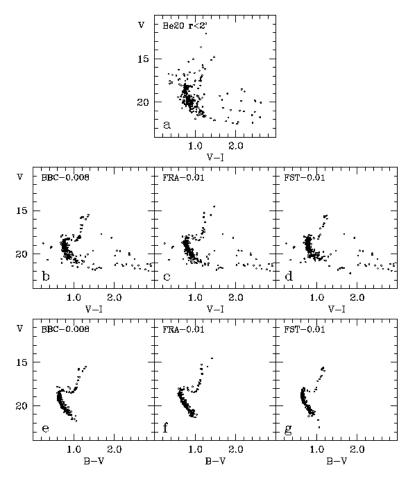


Figure 10. Comparison between observational and synthetic CMDs for Be 20. Panel a shows the stars measured in V, and I in the central 2' radius region. Panels b, c, and d show the synthetic CMDs of best-fitting cases of each type of stellar model, overimposed to the CMD of the same area in the control field for a more direct comparison. Panels e, f, and g show the corresponding B-V CMDs. The displayed cases assume: Z=0.008, age=5.8 Gyr, (m-M)<sub>0</sub>=14.7, E(B-V)=0.13 for BBC, Z=0.01, age=4.3 Gyr, (m-M)<sub>0</sub>=14.7, E(B-V)=0.16 for FRA, and Z=0.01, age=5.0 Gyr, (m-M)<sub>0</sub>=14.7, E(B-V)=0.16 for FST.

as the small number statistics, weakens the discrimination power of the LF comparison. In fact, all the reasonable cases present LFs similar to each other, such as those displayed in Fig. 11. In this plot the dots show the LF of the 269 stars within 2' from the centre of Be 20, and the curves the LF of the (synthetic + field) stars of the CMDs in the central row panels of Fig. 10. The faint portions (dominated by field stars) of all the curves are in good agreement with the empirical LF, while the bright portions are consistent with it, but generally underestimated. We ascribe this underestimation of the number of relatively bright stars both to luminous interlopers and to the possible presence of BSS, not accounted for in the synthetic CMDs.

Our photometry is only in two bands and, by itself, does not allow a reliable identification of the cluster metallicity. Models with solar metallicity or Z=0.004 do not reproduce the CMD morphology as well as models with intermediate metallicity, but cannot be excluded. Since the simultaneous agreement of the synthetic B-V and V-I with the corresponding observational colours is a powerful metallicity indicator (see e.g. Tosi et al. 2007 for King 11), we have overcome our deficiency of information comparing the synthetic V, B-V diagrams with the corresponding CMD published by Durgapal et al. (2001). The self-consistency of this solution is guaranteed by the agreement between our photometry and theirs, shown in Fig. 1. The V, B-V CMD of the stars from

Durgapal et al. (2001) located within 2' from the cluster centre is shown in Fig. 12.

By comparing the synthetic diagrams based on all the stellar evolution sets and on various assumptions on the age, distance and reddening of Be 20 with our V,V-I CMD and with the V,B-V CMD from Durgapal et al. (2001), we are able to distinguish quite well all the cluster parameters. We find that only models with Z=0.008 or 0.01 can simultaneously reproduce the B-V and V-I observed colours. For higher metallicities B-V is always too red when V-I is fine, and, vice versa, for lower metallicities B-V is always too blue when V-I is fine. Hence, we assign to Be 20 a metallicity Z=0.009 $\pm$ 0.001. This photometric estimate of the cluster metallicity is in perfect agreement with that inferred by Sestito et al. (2008) from high-resolution spectroscopy ([Fe/H]=-0.3).

The age providing the best reproduction of the observed CMD morphology and stellar density in the different evolutionary phases depends on the assumptions of the stellar evolution tracks and is therefore slightly different from one set of models to the other. In spite of the field contamination and small number statistics, the clear identification from RVs of the SGB and clump stars allows us to infer the cluster age quite strictly. With the FRA models the age is in the small range 4.3 – 4.5 Gyr: older cases have the clump too bright, and younger cases have it too faint. With overshooting

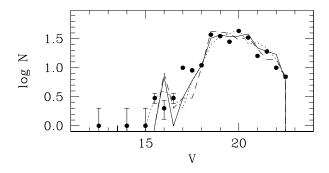


**Figure 11.** Comparison between observational (dots) and synthetic (curves) LFs of the stars within 2' from the centre of Be 20. The curves include the 200 synthetic stars and the 70 stars of the control field, and correspond to the cases shown in Fig. 10: solid for the BBC models, dotted for the FRA and dashed for the FST ones.

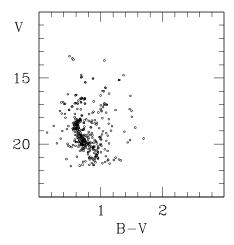


**Figure 12.** V, B - V CMD of stars within 2' from the centre of Be 20, from Durgapal et al (2001).

models, the age is obviously older, but only by less than 25% because in these low mass stars overshooting is not very effective. With the FST models the best-fitting ages are between 5 and 5.5 Gyr, while with the BBC models they are between 5.5 and 5.8 Gyr.

Reddening and distance modulus are also well identified by best-fitting magnitudes and colours of the main evolutionary phases. Particularly striking is the circumstance that all the models in agreement with the data require (m-M) $_0$ =14.7. E(B-V) is more sensitive to the metallicity and the details of the stellar models, and we find it to range between 0.13 (for all the BBC-0.008 good cases) and 0.16 (corresponding to the FRA-0.01 case with age 4.3 Gyr).

In summary, thanks to the cluster membership provided by the radial velocities, age, distance, reddenning and metallicity of Be 20 are very well identified.

# 5.2 Be 66

The situation for Be 66 is apparently more complicated, both because of its high extinction and of the lack of information on membership. The fraction of fore/background contaminating objects doesn't significantly vary from the cluster centre to the periphery and we have therefore chosen to simulate the whole CMD. Since

the stars measured in all the three B,V and I bands are 2362 in our cluster field and 1023 in the control field, the synthetic CMDs have been created with 1339 objects, assuming the photometric errors and the completeness factors described in Sect. 3.

The major problem encountered by all models is the width of the evolutionary sequences, both in colour and in magnitude. In no way are we able to create synthetic diagrams with the observed width by including only photometric errors and binary systems. However, the synthetic sequences become properly thick if we assume variable amounts of reddening. We find that a  $\delta E(B-V)=\pm 0.02$  is sufficient to account for the observed spread. Given the high reddening affecting Be 66, this variation corresponds to only 2-3 per cent and looks rather likely.

The widths of the MSTO, SGB and clump could also make it more difficult to precisely define the cluster parameters. However, it turns out that the independent constraints from the colour, magnitude, morphology, stellar density of the different evolutionary sequences and luminosity function do allow to significantly reduce the range of possible values. The distance modulus, for instance, turns out to be strikingly stable in all the models in acceptable agreement with the data: in spite of its dependence on age, reddening and metallicity, we find  $13.2 \leqslant (m-M)_0 \leqslant 13.5$  in all the acceptable cases, and  $(m-M)_0 = 13.3$  in all the best cases.

To identify the cluster metallicity, the clue is the simultaneous consistency of both the predicted B-V and V-I colours with the observed ones. All the models with solar metallicity and right B-V predict too blue V-I, so we can therefore exclude Z=0.02. For lower metallicity, the different sets of stellar tracks have the following responses: at Z=0.01, the FST models still show the B-V inconsistency with V-I of the solar models, although at a lower level, while the FRA models cannot be excluded. The BBC models with Z=0.008 have self-consistent colours and acceptable CMD and LF properties. The FST models with Z=0.006 perfectly match the observational CMD and LF, and the FRA models with Z=0.006 also have self-consistent colours and accetable CMDs and LFs. Also the BBC models with Z=0.004 give self-consistent colours and acceptable CMDs and LFs. Within the uncertainties, all these results indicate that the metallicity of Be 66 is most likely Z=0.006±0.002. This value corresponds to  $[Fe/H] \simeq -0.45$ , lower than the range proposed by Phelps & Janes (1996) but in perfect agreement with the clump star abundance measured by Villanova et al. (2005) from high resolution spectroscopy.

The reddening resulting from the synthetic CMDs depends both on the adopted models and metallicities. In the cases in better agreement with the data, we find it to range between  $E(B-V)=1.22\pm0.02$  and  $1.30\pm0.02$ , where 0.02 is the variation necessary to reproduce the observed spread of the evolutionary sequences. In the best-fitting case (FST with Z=0.006 and  $\tau$ =3 Gyr) E(B-V)=1.26  $\pm$ 0.02.

The age depends on the various assumptions as well. However, in spite of the width of the evolutionary sequences and the uncertainties on reddening and metallicity, we find it to be rather well determined for each kind of stellar models, thanks to the well defined shape and stellar density of key phases, such as MSTO, SGB, RGB and clump. With the FRA models without overshooting we find  $2.7 \leqslant \tau/Gyr \leqslant 3.0$ , both for Z=0.006 and Z=0.01, with the preferred value between 2.7 and 2.8 Gyr. The models with overshooting provide  $3.5 \leqslant \tau/Gyr \leqslant 4.0$  with the BBC models with either Z=0.004 and Z=0.008 (preferred value 3.8 Gyr), and  $3.0 \leqslant \tau/Gyr \leqslant 3.5$  with the FST models with intermediate overshooting (preferred value 3.0 Gyr).

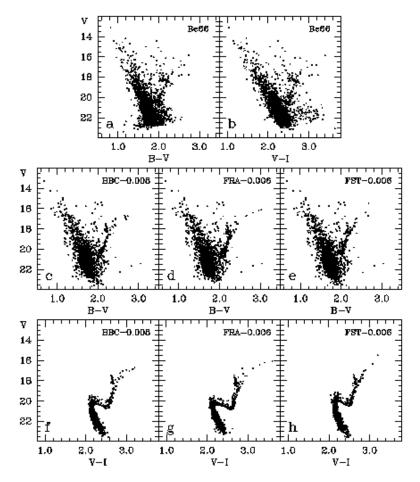
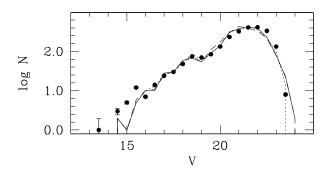


Figure 13. Comparison between observational and synthetic CMDs for Be 66. Panels a and b show the stars measured in B, V, and I in our cluster field. Panels c, d and e show the synthetic V, B-V CMDs of best-fitting cases of each type of stellar model, overimposed to the CMD of the same area in the control field for a more direct comparison. Panels f, g and h show the corresponding V, V-I CMDs. The displayed cases assume: Z=0.008, age=3.8 Gyr, (m-M) $_0$ =13.3, E(B-V)=1.20, 1.22, 1.24 for BBC; Z=0.006, age=2.7 Gyr, (m-M) $_0$ =13.5, E(B-V)=1.28, 1.30, 1.32 for FRA, and Z=0.006, age=3.0 Gyr, (m-M) $_0$ =13.3, E(B-V)=1.24, 1.26, 1.28 for FST.



**Figure 14.** Comparison between observational (dots) and synthetic (curves) LFs of the stars in Be 66. The curves include the 1339 synthetic stars and the 1023 stars of the control field, and correspond to the cases shown in Fig. 13: solid for the BBC models, dotted for the FRA and dashed for the FST ones.

Fig.13 shows the synthetic CMDs in better agreement with the V,B-V and V,V-I diagrams for each set of tracks, selected by minimizing the differences between morphology, star counts, luminosity and colour functions in the observational and synthetic

MS, MSTO, SGB, RGB and clump phases. The two top panels of the Figure show the observational CMDs, the bottom panels show the best synthetic V, V-I CMDs obtained with the BBC, FRA and FST models, while the panels in the central row show the V, B-V CMDs of the same cases as in the bottom row, overimposed to the CMD of the control field stars.

Fig.14 compares the cluster LF with the LFs from the synthetic cases shown in Fig. 13. The three models predict LFs so similar to each other that the three curves overlap almost completely. They all agree very well with the data, except at the bright end, where field contamination dominates and the difference between the foreground stars in the cluster field and in the control field is apparent.

For Be 66, the FST models with Z= 0.006, age=3 Gyr, E(B-V) =1.26±0.02 and  $(m-M)_0$ =13.3 are by far the ones in better agreement with the data.

# 5.3 To 2

As discussed in the previous Sections, To 2 presents a fairly complicated CMDs, strongly affected by (probably multiple) contamination. We did observe a nearby region as control field to evaluate the contamination, but the comparison of its CMD with that

of To 2 clearly shows that the two populations are rather different from each other (see Fig.7). Moreover, we didn't have the opportunity to acquire images of the external field in all the filters, and B is missing. Hence, the control field is of little help to decontaminate To 2. From the morphology of To 2's CMDs with increasing distance from the cluster centre it is apparent that in the circle within 2 arcmin the contamination is still rather significant (at least 15%, according to the number of stars in an equal area region of the control field). To minimize it, we thus decided to adopt as reference cluster CMD that of the central region of 1 arcmin radius (see Fig.8). It contains 1147 objects with measured V and I magnitudes, and 846 with B, V and I. Since control field portions of equal size contain 100 stars with measured V and I, we can assume a 9 percent (lower limit to) contamination. In other words, of the 846 objects with measured BVI, 770 can be considered To 2 members. The synthetic BVI CMDs have been therefore computed assuming this number of objects. The B-V and V-I CMDs of the 846 BVI objects in the central region of To 2 are displayed in the top panels of Fig.15.

Also in this case, we have tried to blindly identify the metallicity, without biassing our search on the basis of literature estimates, for homogeneity with the BOCCE project procedure. All the models clearly exclude a solar metallicity: whatever the adopted tracks, Z=0.02 always lead to CMDs inconsistent with the data both because of the MS shape and of the colours. If we assume a reddening allowing to reproduce the B-V colours, then V-I is systematically too blue, and vice versa. Moreover, the acceptable reddenings are systematically lower than in literature. While rejecting a solar metallicity is straightforward, finding the best fitting one is extremely difficult, because contamination affects key features before and after the MSTO. Since a good identification of the metallicity is necessary to identify the reddening, our analysis leaves the latter rather uncertain too. Vice versa, the distance modulus of To 2 turns out only moderately sensible to the metallicity choice and between 14.4 and 14.7 for any viable model.

With the BBC models, the available metallicity most appropriate for the CMD of To 2 is Z=0.008, whose models allow to self-consistently reproduce the observed B-V and V-I colours of all the evolutionary phases. However, the corresponding upper MS and MSTO regions never have exactly the same morphology as the observed ones. The best CMD with these tracks assumes age  $\tau = 1.6$  Gyr, reddening E(B-V) = 0.34 and distance modulus (m-M)<sub>0</sub>=14.5. Its CMDs are plotted in panels c and d of Fig.15. Panel f shows only the 770 synthetic stars, while panel c contains 846 objects like the empirical CMDs of the top panels, since it includes also the 75 objects falling in an equal area portion of the control field. The comparison of panels b and c emphasizes the difference between the control field and the cluster contaminating stars. BBC models with Z=0.004 also lead to an acceptable self-consistency between B-V and V-I colours, but systematically have RGBs redder and MSs straighter than observed. For this reason we consider them less appropriate for To 2 than the Z=0.008 ones.

For the other types of models, both the FRA and the FST metallicities below solar are Z=0.01 and Z=0.006, and for both it is impossible to significantly discriminate between them. With the FRA models, both metallicities allow for self-consistent colours, but both provide RGB always quite redder than observed. To shrink the subgiant branch and keep the RGB within the observed colour range, one should increase the age, but this inevitably implies clumps brighter than observed. Generally speaking none of the FRA models reproduces adequately the properties of To 2's CMD. In panels d and g of Fig.15 we simply show the case in smaller

disagreement, with no claim of actual consistency. It corresponds to Z=0.006, age 1.4 Gyr, E(B-V)=0.40 and distance modulus (m-M) $_0$ =14.5.

With the FST models, discerning the right metallicity is equally difficult, because Z=0.006 leads to the best self-consistency between B-V and V-I, but predicts RGBs slightly redder than observed, while Z=0.01 has V-I slightly too blue when B-V is correct (a typical signature of a metallicity overestimate), but appropriate RGBs. At variance with the FRA models, the FST ones provide however a good agreement with the empirical CMD, actually better than with any of the other models. Based on the overall properties of the CMD (curvature of the MS, shape of the MSTO and subgiant branch, colour and slope of the RGB, morphology of the clump, number of stars in each of these phases) we ended up preferring the Z=0.01 models. Most likely, the right metallicity (at least within the framework of the FST models) is slightly below this value. In panels e and f we have chosen to show one of the best cases among the FST ones: age 1.7 Gyr, E(B-V)=0.31 and distance modulus (m- $M)_0$ =14.7. Here the choice is rather subjective: an age of 1.6 Gyr (with same metallicity and distance modulus and E(B-V)=0.32), or an age of 1.8 Gyr (with same metallicity, E(B-V)=0.30 and distance modulus (m-M)<sub>0</sub>=14.5) would have been good as well.

Since the FST models come in three overshooting flavours (see Table 7), we have tested them all. As often found for the BOCCE clusters, the FST models with overshooting reproduce the CMD of To 2 much better than those without. In this case, we found no significant difference in the quality of the fit from models with the highest or intermediate overshooting.

We have tested various fractions of unresolved binaries and found that while their presence is clearly required to reproduce the secondary MS seen (see Fig.8) at the right of the main MS both in B-V and in V-I (hence a binary fraction of 0 must be rejected), we don't need to invoke particularly high percentages. A 60% fraction would definitely lead to an excessive blend of the binary and single star MSs and is thus beyond the acceptable value. We conclude that a fraction around 30% provides a good representation of the data.

The difficulty in properly characterizing the field contamination has the further consequence of reducing the selection power of the comparison between synthetic and empirical LF. In Fig.16 the LFs of the three models plotted in panels c, d and e of Fig.15 are plotted as lines, while the empirical LF of the 846 stars of the central 1'of To 2 is represented by dots with error bars. The synthetic LFs fit reasonably well the portions where the cluster dominates, but at both the faint and the bright ends, where contamination dominates and the control field is not representative of that population, all the LFs fail, inevitably unable to predict the number of interlopers. Notice however that in the central parts of the plot, the agreement is fairly good. In particular the bump and dip corresponding to the clump are well fitted, showing that both age and distance modulus are appropriate.

To summarize, we conclude that within the high uncertainties, To 2 turns out to be a cluster of intermediate age (1.4 Gyr for models without overshooting, 1.6-1.8 Gyr for models with overshooting), with distance modulus 14.5-14.7, and with reddening between 0.30 and 0.40 depending on the chosen metallicity, but most likely within 0.31-34 (i.e. for  $0.008 \le Z \le 0.01$ ).

It is interesting to notice that, in spite of the uncertainty in the identification of the best metallicity, we don't find any need of a metallicity spread as found by Frinchaboy et al. (2008). Assuming a metallicity or reddening dispersion in our synthetic CMDs would introduce a spread in the evolutionary sequences larger than observed. Notice that only their metal-poor population falls in the

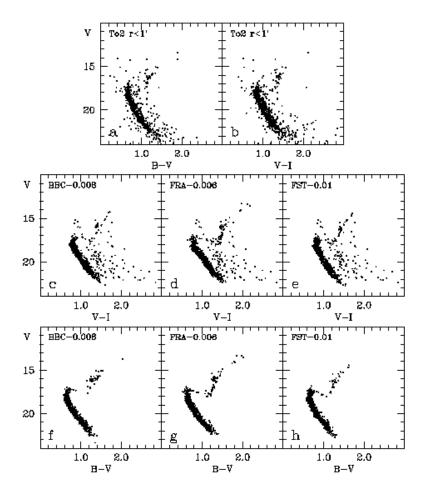
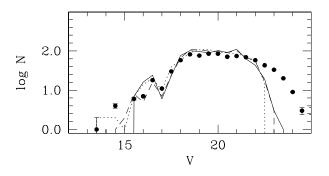


Figure 15. Comparison between observational and synthetic CMDs for To 2. Panels a and b show the stars measured in B, V, and I in the central 1' radius region. Panels c, d, and e show the synthetic CMDs of best-fitting cases of each type of stellar model, overimposed to the CMD of the same area in the control field for a more direct comparison. Panels f, g, and h show only the synthetic stars of the corresponding B - V CMDs. The displayed cases assume: Z=0.008, age=1.6 Gyr, (m-M)<sub>0</sub>=14.5, E(B-V)=0.34 for BBC, Z=0.006, age=1.4 Gyr, (m-M)<sub>0</sub>=14.5, E(B-V)=0.040 for FRA, and Z=0.01, age=1.7 Gyr, (m-M)<sub>0</sub>=14.7, E(B-V)=0.31 for FST.

central 1'-radius circle, so our result of a single population of stars with a single metallicity  $0.008 \leqslant Z \leqslant 0.01$  is in perfect agreement with theirs, as are also reddening and distance modulus. Since in the CMD of the region with 2'-radius we already see significant contamination, and since the most central metal-rich star is at least 1.5' from To2's centre (see their Fig. 2), of the various alternatives examined by Frinchaboy et al. we favour the interpretation of the metal richer populations in terms of an interloper. The more recent finding of absence of any metallicity dispersion (Villanova et al. 2010) is even more easily in agreement with our study. The metallicity is similar, as are the distance, reddening, and age.

# 6 SUMMARY AND DISCUSSION

We compared the CMDs of the three old, distant OCs Be 20, Be 66, and To 2 to synthetic ones based on three different sets of evolutionary tracks and determined the clusters parameters. Table 8 gives a summary of the derived parameters for the three OCs. We use here the values based on the BBC tracks, even when they do not offer the best-fitting solution (e.g., for Be 66), in analogy to what we did



**Figure 16.** Comparison between observational (dots) and synthetic (curves) LFs of the stars within 1' from the centre of To 2. The curves include the 770 synthetic stars and the 76 stars of the control field, and correspond to the cases shown in Fig. 15: solid for the BBC models, dotted for the FRA and dashed for the FST ones.

in Bragaglia & Tosi (2006) to obtain a homogeneous ranking on a single scale.

• All three clusters are less metal-rich than the Sun, with

**Table 8.** Summary of the parameters for the three clusters. We use the BBC results, for homogeneity in ranking and immediate compatibility with the 16 OCs presented in Table 1 of Bragaglia & Tosi (2006); see text for the values derived using the other tracks. Note that Be 66 has differential reddening.

OC	age (Gyr)	$(m - M)_0$	d <sub>⊙</sub> (kpc)	R <sub>GC</sub> (kpc)	E(B-V)	Z
Be 20	5.8	14.7	8.71	16.0	0.13	0.008
Be 66	3.8	13.3	4.57	12.0	1.22	0.008
To 2	1.6	14.5	7.95	14.3	0.34	0.008

best=fitting solutions of Z=0.008-0.01 (depending on the set of tracks) for Be 20 and To 2, and Z=0.006 for Be 66. These rather precise values could be obtained because we considered the simultaneous good fit of both the V-I and B-V CMDs.

- The reddenings slightly depend on the tracks metallicity. For Be 66, we confirm Phelps & Janes (1996)'s suggestion of a probable differential reddening, of the order of 2-3 per cent, a rather likely occurrence given the high extinction level.
- For all clusters a binary fraction of about 30 per cent seems necessary to well reproduce the width of the observed sequences.
- The derived ages depend on the treatment of convection adopted in the evolutionary tracks, with the usual lower values found for tracks without overshooting.
- Our results on age, distance and reddening do not significantly differ from the most recently published ones for Be 20 and To 2. We find Be 66 slightly younger, closer, and definitely metal poorer than Phelps & Janes (1996), while we agree with them on the reddening and with Villanova et al. (2005) on the rather low metallicity.
- As already anticipated in Sect. 1, these OCs have Galactocentric radii of about 12 to 16 kpc and are then useful to constrain the properties of the outer disc, in particular in what seems to be a transition region for the metallicity distribution (see below).

The Galactocentric metallicity gradient - Even if the number of known old OCs has steadily grown in the last years, they still are a minority, since the Dias et al. (2002) catalogue contains about 2000 objects, and only about 190 are older than 1 Gyr (see Fig. 17). An even smaller number of clusters has the metallicity determined using high-resolution spectroscopy (see below). In the BOCCE project we have especially targeted old clusters, hence our OCs represent a fair sample of the old cluster population, about 10 per cent. In Fig. 17 we also show for comparison the same histogram for our sample, <sup>2</sup> and indicate the three clusters analysed here in the enlargement.

The metallicity distribution in the disc is an important ingredient of chemical evolutionary models, and offers essential information on the formation and evolution of the disc, especially when also its possible evolution with time is considered. We may obtain the present-day metallicity distribution from O,B stars and H

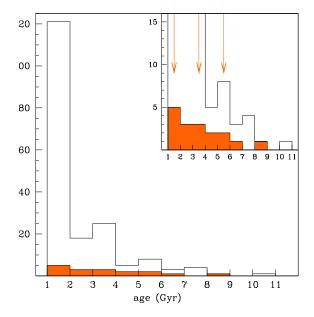


**Figure 17.** Age distribution for the 186 OCs older than 1 Gyr, according to the 2010 update of the Dias et al. (2002) catalogue. The filled histogram represents the 17 clusters in the BOCCE sample within the same age limit (14 already published, three in the present paper). The inset shows an enlargement to better appreciate the -still small- number of very old objects, and the three new OCs are indicated by arrows.

II regions (see, e.g., Rudolph et al. 2006). Another possibility are Cepheids (e.g., Andrievsky et al. 2004), for which the distance and age can be determined with high precision. Planetary nebulae (PNe) are another tracer, and they are in principle able to reach further in the past (see, e.g., the recent paper by Stanghellini & Haywood 2010); however, there still are difficulties in assigning individual ages and distances. This is in general true for all field stars; the most accurate parallaxes to date, those measured by the Hipparcos space mission, are available only for the Sun's vicinity. Ground-based catalogues can reach farther away, but at the price of accuracy. HST parallaxes can be very precise, but only a handful of targets has been observed. To obtain precise distances for hundred millions stars in the whole Galaxy we will have to wait about 10 years, for the completion of the Gaia<sup>3</sup> satellite survey.

Furthermore, all stars are subject to orbit migration (see, e.g., Sellwood & Binney 2002; Roškar et al. 2008; Schönrich & Binney 2009, in the recent years); they move away from their birthplace even several kpc, thus complicating the study of the metallicity distribution: at any given  $R_{GC}$  we may find stars born there, or in an inner (i.e., in general more metal-rich) or in an outer (i.e., in general more metal-poor) region of the disc.

OCs are less subject to all these problems: their distances and ages can be measured with sufficient precision using the stellar models (e.g., as we do in our BOCCE project, see Bragaglia & Tosi 2006), their abundances can be determined from several or many member stars (e.g., Bragaglia et al. 2008), and they do not appear to suffer from orbit migration. For the last point, see e.g., Wu et al. (2009), who computed the orbits of about 500 OCs, using information from Dias et al. (2002). When they derive the slope of the metallicity gradient using  $R_{GC}$  or the apogalacticon radius, they do not find any significant difference. Apart from a few exceptions,

<sup>&</sup>lt;sup>2</sup> This comparison is only indicative, since age determinations are not homogeneous between our work and the catalogue (and inside the catalogue itself). There are differences, sometimes large, between ages measured by different authors. For instance, in Dias et al. (2002), a) one of the two clusters in the last bin -age 10 to 11 Gyr- is Be 17 that, according to Bragaglia et al. (2006a) is instead less than 9 Gyr old, b) King 11 is given an age of 1.1 Gyr, while we derived an age  $\gtrsim$  4 Gyr (Tosi et al. 2007), in line with other determinations, and c) NGC 6791 is attributed an age, 4.4 Gyr, younger than found in all recent papers, where its age is 7-9 Gyr (see, e.g, King et al. 2005).

<sup>&</sup>lt;sup>3</sup> See http://www.rssd.esa.int/index.php?project=GAIA&page=index.

it appears safe to use OCs and their present-day positions, to define the metallicity distribution now and in the past. This is part of our goals, and we are building the BOCCE sample choosing OCs which cover the whole distribution of clusters' properties. Of course, the situation will further improve when it will be possible to compute orbits for the whole family of OCs, using the improved distances, proper motions, and radial velocities produced by Gaia.

We show in Fig. 18(a) the radial metallicity gradient described by OCs using the information in the Dias et al. (2002) catalogue. We computed  $R_{GC}$  using 8 kpc as the Sun distance from the Galactic centre, and the tabulated distances from the Sun. Values for [Fe/H] come from photometry (CMD, narrow-band, indices), low resolution, and high resolution spectroscopy; individual references can be found at the Dias webpage (http://www.astro.iag.usp.br/~wilton/). We display with filled (red) symbols the postion of Be 20, Be 66, and To 2, using the tabulated values. The metallicity tends to decline from the centre to the outskirts of the disc. If we fit the distribution with a single relation, we find a decline rate of  $-0.04 \, \mathrm{dex \, kpc^{-1}}$ , as indicated in the figure. However, recent studies of open clusters (e.g., Yong et al. 2005; Carraro et al. 2007; Sestito et al. 2008; Friel, Jacobson, & Pilachowski 2010) suggest that a better representation is a gradient in the inner region (≤12 kpc from the centre) followed by an almost flat value therefore. We then divided the sample of OCs accordingly, computing a (steeper) inner slope of  $-0.07 \text{ dex kpc}^{-1}$ . The OCs in the external part have in this case an average metallicity of =-0.35 dex. While the number of OCs in this sample is large (177 objects), they tend to lie mostly in the Sun's vicinity, with only about 15 per cent of them with  $R_{GC} > 12$ kpc, and only a handful in the outermost disc regions. Furthermore, the sample is completely inhomogeneous.

In principle, choosing only [Fe/H] measured using high resolution spectroscopy produces more solid results. We have searched the literature and retrieved the metallicity, distance, and age of about 70 clusters. A good fraction of them, about 30 per cent, are also in the BOCCE sample and are indicated with filled symbols in the figure; we show the three clusters of the present paper with larger symbols, this time using the parameters derived in the present paper and the [Fe/H] values indicated in Table 6. We restricted our search to clusters older than 0.1 Gyr and selected in each case either the most recent determination or our measures, when present. The resulting metallicity distribution is shown in Fig. 18(b). The slopes derived are (almost) the same as in the previous case. In this case, however, there is a better balance between inner and outer clusters, and the individual values are more precise (but again, with a caveat on the inhomogeneity of sources, which produces systematics). Be 66, To 2, and Be 20, in order of increasing distance from the centre, are an important addition, since they are about one fifth of the entire outer-disc sample.

This second sample of OCs can also be used to study the behaviour of the gradient with time. In Fig. 19 we divide the sample in three parts and compute the slope of the gradients (only in the inner 12 kpc) again, with the three clusters hightlighted. While young and intermediate age clusters seem to share the same behaviour, the slope of the gradient seems to have been steeper in the past (as found also for PNe). This has to be accounted for by any chemical evolution model. Note however the paucity of very old clusters at the transition between a decreasing and flat distribution of metallicities; this calls for new additions to the well-studied cluster sample.

We plan to repeat these exercises using only clusters in the BOCCE sample, with ages, distances, and [Fe/H] all derived on the same scale. The importance of Be 20, Be 66, and To 2 lies both

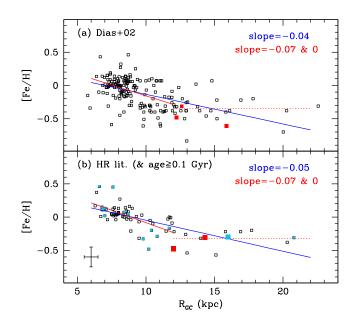


**Figure 18.** The metallcity gradient as defined by OCs. (a)  $R_{GC}$  and [Fe/H] are taken from Dias et al. (2002). The two lines represent the fit to the data using a single slope (in blue) or two, within 12 kpc from the Galactic centre and farther than this limit (in red), see text. The three clusters of the present paper are indicated by filled (red) squares. (b)The same, but using only 72 OCs older than 0.1 Gyr and for which the metallicity has been derived with high-resolution spectroscopy (the three clusters are shown with larger symbols); filled, light-blue squares indicate OCs for which [Fe/H] has been determined by our group.

in their old ages and in their large  $R_{GC}$  (see e.g., the sample map in Bragaglia 2007). Be 66 is the outermost cluster in the second quadrant, while Be 20 and To 2 fill the large gap in  $R_{GC}$  between Be 29 (at 20.8 kpc) and Be 22 (at 14.0 kpc). Notice that in the literature very few clusters have been studied beyond a radius of 16 kpc. For instance, Carraro et al. (2007) list only Be 31, Be 73, Be 25, Saurer 1, and Be 29.

Different interpretations of the two-slopes metallicity distribution are possible, either a normal outcome of disc formation and chemical enrichment (e.g., Carraro et al. 2007; Schönrich & Binney 2009) or satellite accretion in the outer disc (e.g., Yong et al. 2005). The former suggestion likely foresees a continuous radial distribution (even if with different slopes, maybe even zero, in different regions), while the latter implies some inhomogeneity reflecting the satellite impact trajectory. It is then important to have as many clusters as possible outside the critical radius of 12 kpc, and to have them in different quadrants.

We will use the information obtained here, together with the detailed chemical abundances from existing and future high resolution spectroscopic data, to increase the BOCCE set and derive conclusions based on a homogeneous analysis.

# **ACKNOWLEDGEMENTS**

We gratefully acknowledge the use of software written by P. Montegriffo, and of the WEBDA database, created by J.C. Mermilliod, and now operated by E. Paunzen at the Institute for Astronomy of the University of Vienna. We thank Mara Manduchi for her work on To 2. This work has made use of VizieR, operated at CDS, Strasbourg, France, and of NASA's Astrophysics Data System. AB ac-

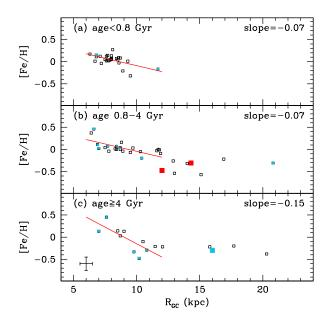


**Figure 19.** The Galactocentric metallicity distribution, in three different time intervals (symbols are as in the previous figure). The slopes, computed only for the inner 12 kpc, are indicated.

knowledges the hospitality of ESO Chile (through the Scientific Visitor Programme) where part of this work was done.

# REFERENCES

Adler D. S., Janes K. A., 1982, PASP, 94, 905

Andreuzzi G., Bragaglia A., Tosi M., Marconi G., 2004, MNRAS, 348, 297

Andrievsky S. M., Luck R. E., Martin P., Lépine J. R. D., 2004, A&A, 413, 159

Bellazzini M., Ibata R., Monaco L., Martin N., Irwin M. J., Lewis G. F., 2004, MNRAS, 354, 1263

Bessell M. S., Castelli F., Plez B., 1998, A&A, 333, 231

Bragaglia A., 2007, arXiv, 711, arXiv:0711.2171

Bragaglia A., 2010, IAUS, 268, 119

Bragaglia A., Tosi M. 2006, AJ, 131, 1544

Bragaglia A., Tosi M., Andreuzzi G., Marconi G., 2006a, MN-RAS, 368, 1971

Bragaglia A., Tosi M., Carretta E., Gratton R. G., Marconi G., Pompei E., 2006b, MNRAS, 366, 1493

Bragaglia A., Sestito P., Villanova S., Carretta E., Randich S., Tosi M., 2008, A&A, 480, 79

Bressan A., Fagotto F., Bertelli G., Chiosi C., 1993, A&AS, 100, 647

Brown J. A., Wallerstein G., Geisler D., Oke J. B., 1996, AJ, 112, 1551

Carraro G., Geisler D., Villanova S., Frinchaboy P. M., Majewski S. R., 2007, A&A, 476, 217

Carretta E., Bragaglia A., Gratton R., D'Orazi V., Lucatello S., 2009, A&A, 508, 695

Davis L. E., 1994, A Reference Guide to the IRAF/DAOPHOT Package, IRAF Programming Group, NOAO, Tucson

Dean J. F., Warren P. R., Cousins A. W. J., 1978, MNRAS, 183, 569

Dias W. S., Alessi B. S., Moitinho A., Lépine J. R. D., 2002, A&A, 389, 871

Di Fabrizio L., Bragaglia A., Tosi M., Marconi G., 2005, MN-RAS, 359, 966

Dominguez I., Chieffi A., Limongi M., Straniero O., 1999, ApJ, 524, 226

Durgapal A. K., Pandey A. K., Mohan V., 2001, A&A, 372, 71 Fagotto F., Bressan A., Bertelli G., Chiosi C., 1994, A&AS, 105, 20

Freeman K., Bland-Hawthorn J., 2002, ARA&A, 40, 487

Friel E. D., 1995, ARA&A, 33, 381

Friel E. D., Jacobson H. R., Pilachowski C. A., 2005, AJ, 129, 2725

Friel E. D., Jacobson H. R., Pilachowski C. A., 2010, AJ, 139, 1942

Friel E. D., Janes K. A., Tavarez M., Scott J., Katsanis R., Lotz J., Hong L., Miller N., 2002, AJ, 124, 2693

Frinchaboy P. M., Majewski S. R., Crane J. D., Reid I. N., Rocha-Pinto H. J., Phelps R. L., Patterson R. J., Muñoz R. R., 2004, ApJ, 602, L21

Frinchaboy P. M., Marino R. R., et al 2008, MNRAS, 391, 39

Frinchaboy P. M., Muñoz R. R., Phelps R. L., Majewski S. R., Kunkel W. E., 2006, AJ, 131, 922

Gratton R., Sneden C., Carretta E., 2004, ARA&A, 42, 385

Ibata R. A., Irwin M. J., Lewis G. F., Ferguson A. M. N., Tanvir N., 2003, MNRAS, 340, L21

Janes K. A., Phelps R. L. 1994, AJ, 108, 1773

Kalirai, J. S., Tosi, M. 2004, MNRAS, 351, 649

King I. R., Bedin L. R., Piotto G., Cassisi S., Anderson J., 2005, AJ, 130, 626

Kubiak M., Kaluzny J., Krzeminski W., Mateo M., 1992, AcA, 42, 155

Landolt A. U., 1992, AJ, 104, 340

MacMinn D., Phelps R. L., Janes K. A., Friel E. D., 1994, AJ, 107, 1806

Martin N. F., Ibata R. A., Bellazzini M., Irwin M. J., Lewis G. F., Dehnen W., 2004, MNRAS, 348, 12

Mermilliod, J.-C. & Paunzen, E., 2003, A&A, 410, 511

Momany Y., et al., 2001, A&A, 379, 436

Momany Y., Zaggia S. R., Bonifacio P., Piotto G., De Angeli F., Bedin L. R., Carraro G., 2004, A&A, 421, L29

Newberg H. J., et al., 2002, ApJ, 569, 245

Ochsenbein F., Bauer P., Marcout J., 2000, A&AS, 143, 23

Panagia N., Tosi M., 1981, A&A, 96, 306

Phelps R. L., Janes K. A., Montgomery K. A., 1994, AJ 107, 1079

Phelps R. L., Janes K. A., 1996, AJ, 111, 1604

Roškar R., Debattista V. P., Quinn T. R., Stinson G. S., Wadsley J., 2008, ApJ, 684, L79

Rudolph A. L., Fich M., Bell G. R., Norsen T., Simpson J. P., Haas M. R., Erickson E. F., 2006, ApJS, 162, 346

Schönrich R., Binney J., 2009, MNRAS, 396, 203

Sellwood J. A., Binney J. J., 2002, MNRAS, 336, 785

Sestito P., Bragaglia A., Randich S., Pallavicini R., Andriewsky S.M., Korotin S.A., 2008, A&A, 488, 943

Stanghellini L., Haywood M., 2010, ApJ, 714, 1096

Stetson P. B., 1987, PASP 99, 191

Tombaugh C., 1938, PASP, 50, 171

Tosi M., Greggio L., Marconi G., Focardi P., 1991, AJ, 102, 951

Tosi M., Bragaglia A., Cignoni M., 2007, MNRAS, 378, 730

Twarog B. A., Anthony-Twarog B. J., 1989, AJ, 97, 759

Twarog B. A., Ashman K. M., Anthony-Twarog B. J., 1997, AJ, 114, 2556

Ventura P., Zeppieri A., Mazzitelli I., D'Antona F., 1998, A&A, 334, 953

Villanova S., Carraro G., Bresolin F., Patat F., 2005, AJ, 130, 652 Villanova S., Randich S., Geisler D., Carraro G., Costa E., 2010, A&A, 509, A102

Yong D., Carney B. W., Teixera de Almeida M. L., 2005, AJ, 130, 597

Wu Z.-Y., Zhou X., Ma J., Du C.-H., 2009, MNRAS, 399, 2146